J. Fluid Mech. (1994), *vol.* 269, *pp.* 107–141

Theoretical analysis of inertially irrotational and solenoidal flow in two-dimensional radial-flow pump and turbine impellers with equiangular blades

By F. C. VISSER, J. J. H. BROUWERS AND R. BADIE
Faculty of Mechanical Engineering, University of Twente, PO Box 217, 7500 AE Enschede, The Netherlands

(Received 1 April 1993 and in revised form 18 December 1993)

Using the theory of functions of a complex variable, in particular the method of conformal mapping, the irrotational and solenoidal flow in two-dimensional radial-flow pump and turbine impellers fitted with equiangular blades is analysed. Exact solutions are given for the fluid velocity along straight radial pump and turbine impeller blades, while for logarithmic spiral pump impeller blades solutions are given which hold asymptotically as $(r_1/r_2)^n \to 0$, in which r_1 is impeller inner radius, r_2 is impeller outer radius and n is the number of blades. Both solutions are given in terms of a Fourier series, with the Fourier coefficients being given by the (Gauss) hypergeometric function and the beta function respectively. The solutions are used to derive analytical expressions for a number of parameters which are important for practical design of radial turbomachinery, and which reflect the two-dimensional nature of the flow field. Parameters include rotational slip of the flow leaving radial impellers, conditions to avoid reverse flow between impeller blades, and conditions for shockless flow at impeller entry, with the number of blades and blade curvature as variables. Furthermore, analytical extensions to classical one-dimensional Eulerian-based expressions for developed head of pumps and delivered work of turbines are given.

1. Introduction

Computing the two-dimensional potential flow in radial-flow impellers, in particular by using the theory of functions of a complex variable, is not a recent development but has been done by a number of notable authors since the early years of this century. It was Kucharski (1918) who pioneered this field of fluid dynamics by thoroughly examining the flow field of a simplified impeller fitted with straight radial blades with the inner tip placed at the centre of the impeller. Spannhake (1925*a*, *b*, 1930) presented improvements by taking a more realistic inlet-to-outlet radius for the impeller, and introduced the method of conformal mapping to solve the flow problem. Employing the method of conformal mapping Sörensen (1927), Busemann (1928), and Schulz (1928*a*, *b*) treated the impeller with logarithmic spiral blades. Here Schulz developed and subsequently used a rather dubious alternative mapping, in that it violated the conservation of flux and circulation. Sörensen and Busemann based their study correctly on the work of König (1922). Uchimaru & Kito (1931) unfortunately applied the (questionable) results of Schulz to compute slip coefficients. Acosta (1954) extended

the work of Busemann by computing the pressure distribution along the blades, and compared the results with experiments. Ayyubi & Rao (1971), and Mohana Kumar & Rao (1977) used Acosta's work as reference and developed similar results by using a distribution of elementary singularities on the blade surfaces.

The above-mentioned authors all contributed significantly to the solution of the potential flow problem in two-dimensional radial-flow impellers. However, results were mostly obtained by numerical evaluation and computation; solutions in closed form were limited to special cases only (Kucharski 1918; Spannhake 1925*a*). This situation is improved by the results of the present paper, that is solutions in closed form are given for a number of important flow parameters which determine the performance of (two-dimensional) radial-flow impellers with equiangular blades. The results given provide an extension to formulae commonly applied at the preliminary design stage in the engineering of radial turbomachinery, such formulae being largely based on the application of one-dimensional Eulerian flow theory. Furthermore, the presented solutions can serve as a practical and meaningful reference for numerical methods used for complex, two- and quasi-three-dimensional, potential flow calculations (see for instance Badie 1993).

2. Formulation

A single-stage turbomachine, or one stage of a multistage turbomachine, may be considered to be composed of three main parts: a stationary inlet or guidance system, the runner or impeller, and an outlet or collecting device. Since the impeller is responsible for the energy transfer, it seems clear that this component should be our first item of interest. Thus confining our attention to the flow field in isolated impellers, it would be highly desirable to be able to predict the developed head or the delivered work, and to determine the fluid velocity and the pressure distribution along the blades. This, however, is in general not feasible due to the behaviour of real fluids, and the complex geometries of impellers found in practice. Therefore the flow problem has to be simplified, leaving the essentials intact, so that practical solutions can be obtained.

The first assumption is that the fluid may be considered incompressible when dealing with pumps, fans, and hydraulic turbines. Secondly, the importance of the viscous forces compared to the non-viscous (inertia) forces acting on the fluid will be very small, so that the bulk of the fluid may be considered inviscid. The third assumption, usually implicitly made, is that the flow enters the impeller free from vorticity, so that the flow field may be characterized mathematically as irrotational and solenoidal taking into account the former two assumptions. The last assumption is that the flow field may be considered two-dimensional, that is the flow is restricted to depend on radial and angular coordinates only. This is a reasonable assumption for numerous radial-flow turbomachines, having a low specific speed (see for instance Pfleiderer 1991).

The above-mentioned assumptions make it possible to use two-dimensional methods of potential flow theory, in particular the theory of functions of a complex variable, to compute the flow in radial-flow impellers. We additionally adopt equiangular blades, that is blades having a constant angle between radius and tangent. These blades are not only mathematically convenient, but also highly representative since most blade designs in practice are closely represented by equiangular blades. Furthermore, the analysis will be restricted to thin blades, that is blades with zero thickness.

So, in brief, the impellers considered are isolated, two-dimensional, of the radial-flow type, and consist of a finite number of negligibly thin, equally spaced, equiangular

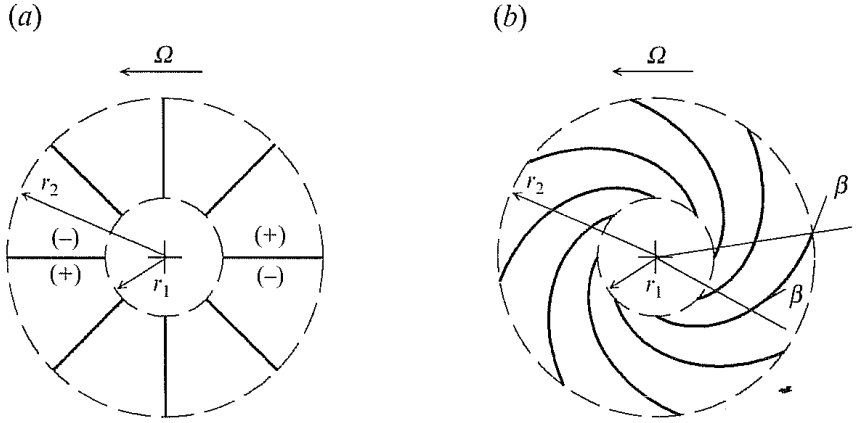

FIGURE 1. Two-dimensional radial-flow impellers. (*a*) Straight radial blades ($\beta = 0$); (*b*) logarithmic spiral blades with $\beta = \frac{1}{3}\pi$.

blades. The coinciding upper (+) and lower (−) blade surfaces of such impellers (see figure 1) are characterized mathematically by

$$r\frac{\mathrm{d}\phi}{\mathrm{d}r} = \tan(\beta) = \text{constant}, \tag{2.1}$$

where r is radial distance and ϕ is polar angle. The blade angle β is constant for all radii and is taken counterclockwise positive (where $0 < \beta < \frac{1}{2}\pi$). The direction of revolution of the impeller, rotating with angular speed Ω, can be either clockwise (i.e. $\Omega < 0$) or counterclockwise (i.e. $\Omega > 0$), representing backward or forward curvature respectively.

Integration of (2.1) yields that equiangularly bladed impellers are described by e.g.

$$\phi^j(r) = \phi_{o1} + 2\pi\frac{j-1}{n} + \tan(\beta)\ln\left(\frac{r}{r_2}\right) \tag{2.2}$$

or

$$r^j(\phi) = r_2\,\mathrm{e}^{-2\pi(j-1)/(n\tan(\beta))}\,\mathrm{e}^{(\phi-\phi_{o1})/\tan(\beta)}, \tag{2.3}$$

in which n is the number of blades, j is the blade index $\{j \in \mathbb{N} \mid 1 \leqslant j \leqslant n\}$, ϕ_{o1} is the offset angle, namely $\phi_{o1} = \phi^1(r_2)$, r_2 is the outer tip radius, and $r_1 \leqslant r \leqslant r_2$ where r_1 is the inner tip radius.

For $\beta \neq 0$ we generally speak of logarithmic spiral blades (see figure 1*b*), whereas straight radial blades are characterized by a blade angle equal to zero. Putting $\beta = 0$ in (2.2) we obtain that straight radial blades are described by

$$\phi^j = \phi_{o1} + 2\pi\frac{j-1}{n}. \tag{2.4}$$

Next, for the flow field in the impeller, which is considered two-dimensional, inertially irrotational, and solenoidal, a velocity potential φ and a stream function ψ can be defined, as is customary in general fluid dynamics, see for instance Batchelor (1967) or Lamb (1932). The complex potential $(\varphi + \mathrm{i}\psi)$ associated with this flow will be denoted by $f(z)$ where $z = x + \mathrm{i}y$, with x and y referring to non-rotating Cartesian (x, y)-coordinates, and, hence,

$$\frac{\mathrm{d}f}{\mathrm{d}z} = v_x - \mathrm{i}v_y, \tag{2.5}$$

where v_x and v_y are the (absolute) velocity components in the x- and y-directions. Furthermore, for convenience in algebraic manipulation, we will distinguish the following potentials:

(*a*) A potential f_Ω due to the rotation of the impeller. This flow will be referred to as displacement flow.

(*b*) A potential f_Q representing the volume flow rate through the impeller, which is incorporated by a source placed at the centre of the impeller; for turbines the source will have a negative strength.

(*c*) A potential f_Γ related to a rectilinear vortex placed at the centre of the impeller. This vortex represents either a prerotation by which we can impose shockless entry for pump impellers, or merely the circulation of the flow leaving turbine impellers.

(*d*) A potential f_K for the imposition of the Kutta condition (or Zhukovski's hypothesis). This condition, being set by the effect of viscosity, expresses the physical fact that there is a smooth flow off both surfaces of the impeller blades at the trailing edge.

3. Method of solution

To solve the flow field, in particular the fluid velocity along the blades, we will employ a conformal transformation which maps the impeller on the unit circle. In the circle plane we can easily determine the previously mentioned sub-flows, by using the theory of functions of a complex variable.

The mapping function is originally credited to König (1922), and originates from the transformation of a plane source–vortex flow to a source–vortex flow in a circle plane, see also Acosta (1954), Betz (1964, pp. 245–255), or Busemann (1928). Denoting the physical plane by z and the image plane by ζ and placing the centre of the impeller at the origin in $z = 0$, we can state the transformation ζ: $z \to \zeta$, which maps the impeller conformally on the unit circle, as

$$\left(\frac{z}{z_2}\right)^n = \left(\frac{\zeta-\zeta_0}{\zeta_2-\zeta_0}\right)\left(\frac{\dfrac{1}{\zeta}-\bar{\zeta}_0}{\dfrac{1}{\zeta_2}-\bar{\zeta}_0}\right)^{e^{2i\beta}}, \tag{3.1}$$

in which $\zeta_0 = \zeta(0)$ and $\zeta_2 = \zeta(z_2)$, with z_2 being the complex representation of the outer blade tip in the physical plane, and where the overbar denotes the complex conjugate.

An alternative transformation which maps the impeller on the unit circle is due to Schulz (1928*a*, *b*). Schulz' transformation, employed also by Uchimaru & Kito (1931), may be written as

$$\left(\frac{z}{z_2}\right)^n = \left(\frac{\zeta-\zeta_0}{\zeta_2-\zeta_0}\,\frac{\dfrac{1}{\zeta}-\bar{\zeta}_0}{\dfrac{1}{\zeta_2}-\bar{\zeta}_0}\right)^{e^{i\beta}/\cos(\beta)}. \tag{3.2}$$

This transformation partially resembles transformation (3.1) and, moreover, is relatively simple. Unfortunately, transformation (3.2) violates the conservation of flux and circulation, and therefore it is unsuited for solving the irrotational and solenoidal flow field; the physical nature of sources and vortices is affected illegally by transformation (3.2), that is sources and vortices are both transformed in vortex-

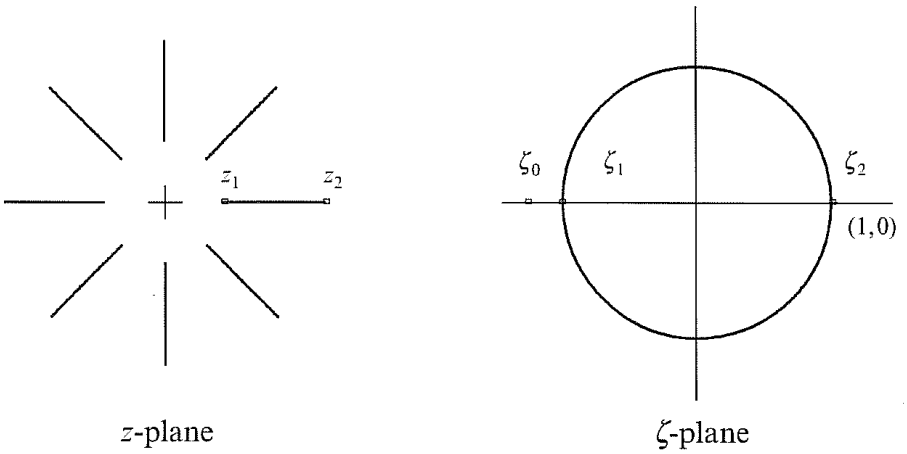

FIGURE 2. Mapping of eight straight radial blades.

sources. In fact, this is a rather logical consequence of Schulz' approach, because Schulz transforms a plane vortex–source flow to a source flow in the circle plane. Transformation (3.1) is the proper one to use.

Mapping the impeller according to transformation (3.1) we still have a degree of freedom left, namely the exact location of the image ζ_0 of the origin ($z = 0$) of the physical plane. This image ζ_0 may either be taken freely, or it may be derived from a chosen image ζ_2. The latter will be done for both straight radial blades and logarithmic spiral blades.

3.1. *Mapping function for straight radial blades (figure 2)*

Putting $\beta = 0$, choosing the image of the outer blade tip in $\zeta_2 = 1$, and employing the fact that the blade tips are branch points of the transformation, which implies $|\mathrm{d}z/\mathrm{d}\zeta|_{\zeta_1,\zeta_2} = 0$, it follows from (3.1) that the inner blade tip is mapped in $\zeta_1 = -1$, and that the image of the origin ($z = 0$) lies somewhere on the negative real axis, say $\zeta_0 = -a$ with $a \in \mathbb{R}^+$, see also Betz (1964, pp. 123–131) or Spannhake (1925*a*, 1930). The mapping function (3.1) then becomes

$$\left(\frac{z}{z_2}\right)^n = \frac{(a+\zeta)(a+(1/\zeta))}{(1+a)^2}. \tag{3.3}$$

Next, defining

$$\mu = (r_1/r_2)^n \tag{3.4}$$

and taking into account that the physical plane is mapped outside the unit circle, so that $a > 1$, it follows that

$$a = (1+\mu^{\frac{1}{2}})/(1-\mu^{\frac{1}{2}}). \tag{3.5}$$

For points on a blade, i.e. $\zeta = \mathrm{e}^{\mathrm{i}\theta}$ and $z = r\,\mathrm{e}^{\mathrm{i}\phi'}$, the mapping function (3.3) becomes

$$\{R(\theta)\}^n = \frac{1+\mu}{2}\left(1+\frac{1-\mu}{1+\mu}\cos(\theta)\right), \tag{3.6}$$

where we have introduced a dimensionless radius

$$R(\theta) = r(\theta)/r_2, \tag{3.7}$$

which will be used frequently henceforth.

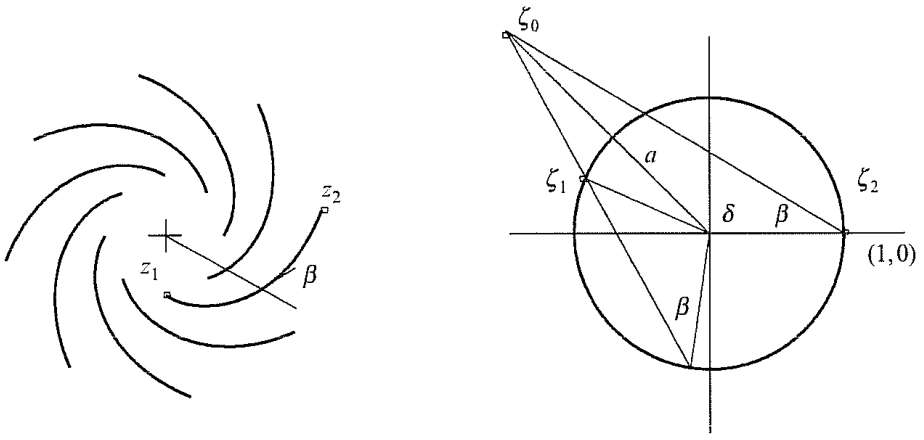

FIGURE 3. Mapping of eight logarithmic spiral blades with $\beta = \frac{1}{3}\pi$.

3.2. *Mapping function for logarithmic spiral blades (figure 3)*

Putting $\zeta_0 = a\,e^{i\delta}$ in transformation (3.1), choosing again $\zeta_2 = 1$, and employing the fact that the blade tips are branch points of the transformation, it follows that, see also Acosta (1954) or Busemann (1928),

$$a = \sin(\beta)/\sin(\delta+\beta) \tag{3.8}$$

and that the argument (δ) of ζ_0 is given implicitly by

$$\mu = \left(-\frac{\sin(2\beta+\delta)}{\sin(\delta)}\right)^{2\cos^2(\beta)} e^{-2(\pi-\beta-\delta)\sin(2\beta)}. \tag{3.9}$$

The mapping constants a and δ, as given by (3.8) and (3.9), are rather awkward to compute. However, since $\mu \ll 1$ for most impellers found in practice (e.g. $r_1 = 37$ mm, $r_2 = 100$ mm, and $n = 8$ blades gives $\mu \approx 3.5 \times 10^{-4}$) we may employ a simple approximation. Physically, this approximation embodies small blade space–chord ratios.

From (3.9) it follows that $\delta \sim \pi - 2\beta$ as $\mu \to 0$, taking into account that $a \geqslant 1$ in (3.8). Hence we put

$$\delta = \pi - 2\beta + \varepsilon, \tag{3.10}$$

in which $\varepsilon \sim 0$ as $\mu \to 0$. Then substituting (3.10) in (3.8) and (3.9) we obtain

$$a \sim 1 + \varepsilon \operatorname{cotan}(\beta), \tag{3.11}$$

where

$$\varepsilon \sim (\mu^{\frac{1}{2}})^{1/\cos^2(\beta)} \sin(2\beta)\, e^{2\beta\tan(\beta)} \tag{3.12}$$

as $\mu \to 0$.

Equations (3.10), (3.11), and (3.12) provide a simple algorithm to compute the mapping constants, a and δ, asymptotically as $\mu \to 0$.

Lastly, as a special and highly representative case, the limiting value $\mu \to 0$ will be considered; here we will confine ourselves to the mapping of points located on a blade, which are represented by (2.2) and (2.3). For these points transformation (3.1) may be stated alternatively as, see also Busemann (1928),

$$\{R(\theta)\}^{n/\cos(\beta)} = \omega\bar{\omega} = |\omega|^2, \tag{3.13}$$

in which
$$\omega = \omega(\theta) = \left(\frac{\zeta-\zeta_0}{1-\zeta_0}\right)^{e^{-i\beta}} = \left(\frac{e^{i\theta}-a\,e^{i\delta}}{1-a\,e^{i\delta}}\right)^{e^{-i\beta}}. \tag{3.14}$$

Then, with $a \sim 1$ and $\delta \sim \pi - 2\beta$ as $\mu \to 0$ mapping function (3.13) becomes

$$R(\theta) \sim \left(\frac{\cos(\beta+\frac{1}{2}\theta)}{\cos(\beta)}\right)^{2\cos^2(\beta)/n} e^{\frac{1}{2}\theta \sin(2\beta)/n} \tag{3.15}$$

as $\mu \to 0$, which is valid for $-\pi-2\beta \leqslant \theta \leqslant \pi-2\beta$ and $0 \leqslant \beta \leqslant \frac{1}{2}\pi$. Equation (3.15), like (3.6) being appropriate for straight radial blades, formulates the mapping of points located on logarithmic spiral blades explicitly. Consequently, it is possible to obtain solutions in closed form for the flow problem considered. In particular, the fluid velocity along impeller blades can be solved elegantly in closed form.

4. Flow along the blades

Since important impeller characteristics, such as developed head and delivered work, can be obtained directly from the description of the tangential flow along the blades, our attention will be confined to this flow; a full description, with the aid of solutions in closed form, of the complete flow between the blades is most unlikely to be found because of its complexity. Descriptions of the individual contributions to the tangential velocity along the impeller blades will be derived from the corresponding descriptions of the sub-flows in the circle plane or ζ-plane.

4.1. *Displacement flow*

With reference to figure 4 it follows that the fluid velocity tangential at the blades, due to the displacement flow, is given by Poisson's (principal value) integral, see for instance Betz (1964, p. 167) or Moretti (1964, pp. 280–281)

$$v^{\Omega}_{t\zeta}(\theta) = \frac{1}{2\pi}\int_{\delta-2\pi}^{\delta} v^{\Omega}_{n\zeta}(\lambda)\,\mathrm{cotan}\,(\tfrac{1}{2}\theta-\tfrac{1}{2}\lambda)\,\mathrm{d}\lambda, \tag{4.1}$$

in which the subscripts n and t denote the normal and tangential parts respectively, and where ζ refers to the ζ-plane; the superscript Ω is added to denote the displacement flow.

The normal velocity $v^{\Omega}_{n\zeta}$ in (4.1) follows from the transformation

$$v^{\Omega}_{n\zeta} = v^{\Omega}_{nz}\left|\frac{\mathrm{d}z}{\mathrm{d}\zeta}\right| \tag{4.2}$$

in which the normal velocity v^{Ω}_{nz} is prescribed by the physical fact that, at the blades, the relative fluid velocity normal to the blades equals zero. By this boundary condition it follows that

$$v^{\Omega}_{nz} = (\boldsymbol{\Omega} \times \boldsymbol{r})\cdot \boldsymbol{n}, \tag{4.3}$$

where $\boldsymbol{\Omega}$ is angular speed of the impeller, $\boldsymbol{r}$ is the position vector for blade-located points, and $\boldsymbol{n}$ is the unit normal of the blade(s). In two dimensions and for equiangular blades (4.3) yields

$$v^{\Omega}_{nz} = (\pm)\,\Omega r \cos(\beta) \tag{4.4}$$

in which $\Omega = |\boldsymbol{\Omega}|$, $r = |\boldsymbol{r}|$, and where the sign $(\pm)$ depends on the side of the blade, that is, $(+)$ for upper and $(-)$ for lower blade surfaces, due to the changing of $\boldsymbol{n}$.

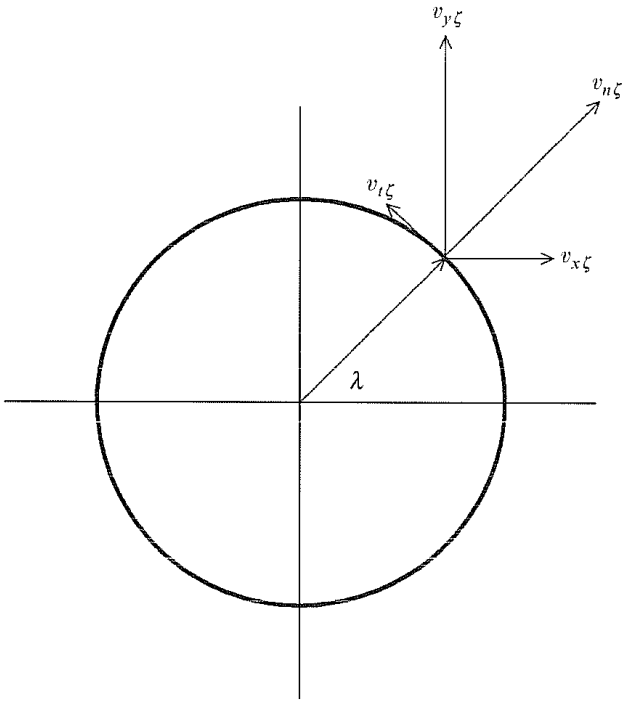

FIGURE 4. Fluid velocities along the unit circle in the ζ-plane.

By some geometrical manipulations it further follows that the derivative of the mapping for points located on equiangular blades may be written as

$$\left|\frac{\mathrm{d}z}{\mathrm{d}\zeta}\right| = (\mp)\frac{1}{\cos(\beta)}\frac{\mathrm{d}r}{\mathrm{d}\theta}, \tag{4.5}$$

the sign $(\mp)$ again depending on the side of the blade. Substituting this result and (4.4) in (4.2) we get, employing the dimensionless radius $R(\theta) = r(\theta)/r_2$,

$$v_{n\zeta}^{\Omega}(\theta) = -\Omega r_2^2 R(\theta)\frac{\mathrm{d}R}{\mathrm{d}\theta}. \tag{4.6}$$

Then, substituting (4.6) in (4.1) we obtain that the fluid velocity along the unit circle, due to the revolution of the impeller, is given by

$$v_{t\zeta}^{\Omega}(\theta) = -\frac{\Omega r_2^2}{2\pi}\int_{\delta-2\pi}^{\delta} R(\lambda)\frac{\mathrm{d}R}{\mathrm{d}\lambda}\operatorname{cotan}(\tfrac{1}{2}\theta-\tfrac{1}{2}\lambda)\,\mathrm{d}\lambda. \tag{4.7}$$

The transformation

$$v_{tz} = v_{t\zeta}\frac{\cos(\beta)}{r_2}\left|\frac{\mathrm{d}R}{\mathrm{d}\theta}\right|^{-1} \tag{4.8}$$

then gives the corresponding (tangential) fluid velocity in the physical plane.

4.2. *Source flow*

Placing a fluid source of strength Q/n in the ζ-plane at $\zeta = \zeta_0$, which corresponds with a fluid source of strength Q located at the centre of the z-plane, yields the potential

$$f_Q(\zeta) = \frac{Q}{2\pi n}\ln(\zeta-\zeta_0). \tag{4.9}$$

Applying the circle theorem of Milne–Thomson (1958) we impose the boundary condition that the unit circle has to be a streamline, and obtain from (4.9)

$$f_Q^*(\zeta) = \frac{Q}{2\pi n}\left(\ln(\zeta-\zeta_0)+\ln\left(\frac{1}{\zeta}-\bar{\zeta}_0\right)\right), \tag{4.10}$$

where the asterisk is added for clarity. Next taking the derivative of (4.10) with respect to ζ, substituting $\zeta = e^{i\theta}$ and $\zeta_0 = a\,e^{i\delta}$, and using the identity

$$v_{x\zeta}(\theta) - iv_{y\zeta}(\theta) = e^{-i\theta}(v_{n\zeta}(\theta) - iv_{t\zeta}(\theta)) \tag{4.11}$$

we get the normal and tangential parts of the fluid velocity along the unit circle due to the source, i.e.

$$v_{n\zeta}^Q(\theta) = 0, \tag{4.12}$$

$$v_{t\zeta}^Q(\theta) = \frac{Q}{\pi n}\frac{a\sin(\theta-\delta)}{1+a^2-2a\cos(\theta-\delta)}. \tag{4.13}$$

Equation (4.12) confirms that the boundary condition is imposed properly. The tangential fluid velocity (v_{tz}^Q) in the physical plane again follows from transformation (4.8).

4.3. *Vortex flow*

Placing a rectilinear vortex of strength Γ_1/n in the ζ-plane at $\zeta = \zeta_0$ yields the potential

$$f_\Gamma(\zeta) = \frac{\Gamma_1}{2\pi n}\ln(\zeta-\zeta_0). \tag{4.14}$$

Applying the circle theorem, (4.14) gives

$$f_\Gamma^*(\zeta) = \frac{\Gamma_1}{2\pi n}\left(\ln(\zeta-\zeta_0)-\ln\left(\frac{1}{\zeta}-\bar{\zeta}_0\right)\right). \tag{4.15}$$

Next taking the derivative of (4.15) with respect to ζ, substituting $\zeta = e^{i\theta}$ and $\zeta_0 = a\,e^{i\delta}$, and using identity (4.11) we find that the normal and tangential parts of the fluid velocity along the unit circle due to the vortex are given by

$$v_{n\zeta}^\Gamma(\theta) = 0, \tag{4.16}$$

$$v_{t\zeta}^\Gamma(\theta) = \frac{\Gamma_1}{\pi n}\frac{1-a\cos(\theta-\delta)}{1+a^2-2a\cos(\theta-\delta)}. \tag{4.17}$$

Again it is seen that the boundary condition is imposed properly. The tangential fluid velocity (v_{tz}^Γ) in the physical plane again follows from transformation (4.8).

4.4. *Kutta condition or Zhukovski's hypothesis*

The last sub-flow to be discussed is related to the Kutta condition, also known as Zhukovski's hypothesis, which implies the elimination of the singular behaviour of the fluid velocity at the trailing edge of a blade. This is done by superposing a rectilinear vortex of strength Γ_b at the origin of the ζ-plane. This additional flow satisfies both the potential equation and the boundary condition that the unit circle is a streamline; the potential reads

$$f_K(\zeta) = \frac{\Gamma_b}{2\pi}\ln(\zeta), \tag{4.18}$$

where Γ_b is the blade circulation, which is (to be) determined by the Kutta condition, and K refers to the Kutta condition.

Taking the derivative of (4.18) with respect to ζ, substituting $\zeta = e^{i\theta}$, and using identity (4.11), gives the normal and tangential parts of the fluid velocity along the unit circle due to the additional vortex Γ_b, i.e.

$$v_{n\zeta}^K = 0, \tag{4.19}$$

$$v_{t\zeta}^K = \Gamma_b/2\pi. \tag{4.20}$$

Now by simply requiring a zero (overall) fluid velocity at the trailing edge in the ζ-plane we impose the Kutta condition. This method will be valid if the decrease of the fluid velocity exceeds the increase of the derivative $(d\zeta/dz)$ of the mapping near the trailing edge.

When imposing the Kutta condition we have to distinguish pumps from turbines because the trailing edges of radial pump impellers lie at the outer radius whereas inward-flow radial turbine impellers have trailing edges at the inner radius.

Imposing the Kutta condition at the outer tip (i.e. $\theta = 0$) yields the relation

$$v_{t\zeta}^{\Omega}(0) + v_{t\zeta}^{Q}(0) + v_{t\zeta}^{\Gamma}(0) + v_{t\zeta}^K = 0. \tag{4.21}$$

Substituting (4.20) in (4.21) we obtain that the blade circulation (Γ_{bp}) for *pump* impellers is given by

$$\Gamma_{bp} = -2\pi(v_{t\zeta}^{\Omega}(0) + v_{t\zeta}^{Q}(0) + v_{t\zeta}^{\Gamma}(0)). \tag{4.22}$$

Imposing the Kutta condition at the inner tip ($\theta = \theta_1$) we analogously obtain for the blade circulation (Γ_{bt}) of *turbine* impellers

$$\Gamma_{bt} = -2\pi(v_{t\zeta}^{\Omega}(\theta_1) + v_{t\zeta}^{Q}(\theta_1) + v_{t\zeta}^{\Gamma}(\theta_1)). \tag{4.23}$$

When turbines are considered, the inner circulation Γ_1 is not prescribed, as it is for pumps, but instead the outer circulation Γ_2 is prescribed. Both circulations are simply related by

$$\Gamma_2 = \Gamma_1 + \sum_{j=1}^{n} \Gamma_b^j, \tag{4.24}$$

where we have omitted the subscripts p (pump) and t (turbine) since (4.24) is universally valid. Alternatively, recalling that we are dealing with isolated impellers, having blade-to-blade-equivalent blade circulations due to the periodicity of the flow, (4.24) may also be stated as

$$\Gamma_2 = \Gamma_1 + n\Gamma_b. \tag{4.25}$$

4.5. *Condition of shockless entry*

After imposing the Kutta condition still another singularity remains, namely the one at the leading edge of the blades. Analogous to the imposition of the Kutta condition this singularity can be eliminated, in this case by a proper choice of the prerotation. This is generally known as (imposing) the condition of shockless entry. This condition of shockless entry is strictly an operating condition, whereas the Kutta condition is a physical fact. From a mathematical point of view, however, both conditions are alike.

When imposing this condition a distinction has again to be made between radial pump impellers and inward-flow radial turbine impellers because of the transposition of the leading edge.

For pump impellers, i.e. the inner tip ($\theta = \theta_1$) as leading edge, the condition of shockless entry yields the relation

$$v_{t\zeta}^{\Omega}(\theta_1) + v_{t\zeta}^{Q}(\theta_1) + v_{t\zeta}^{\Gamma}(\theta_1) + v_{t\zeta}^K = 0. \tag{4.26}$$

Substituting (4.20) in (4.26) and using (4.22) then gives

$$v^{\Omega}_{t\xi}(\theta_1)-v^{\Omega}_{t\xi}(0)+v^{Q}_{t\xi}(\theta_1)-v^{Q}_{t\xi}(0)+v^{\Gamma}_{t\xi}(\theta_1)-v^{\Gamma}_{t\xi}(0)=0. \tag{4.27}$$

Equation (4.27) fully determines the prerotation Γ_{1s} of the flow entering pump impellers, such that a shockless entry is obtained.

For turbine impellers, i.e. the outer tip ($\theta = 0$) as leading edge, the condition of shockless entry yields the relation

$$v^{\Omega}_{t\xi}(0)+v^{Q}_{t\xi}(0)+v^{\Gamma}_{t\xi}(0)+v^{K}_{t\xi}=0. \tag{4.28}$$

Substituting (4.20) in (4.28), and using (4.23) we obtain (4.27) again. This equation indirectly determines the shockless prerotation Γ_{2s} for turbine impellers. Having solved Γ_1 from (4.27) the prerotation Γ_{2s} is next obtained using (4.24).

5. Solutions in closed form for radially bladed pump and turbine impellers

In this section our attention will be confined to the case of straight radial blades. Solutions in closed form for both pump and turbine impellers will be presented, having outlined the universal solutions first.

Putting $\beta = 0$, $\delta = \pi$, and using (3.5) and (3.6), we obtain from (4.7), (4.13), and (4.17)

$$v^{\Omega}_{t\xi}(\theta)=\frac{K}{2\pi n}\int_{-\pi}^{\pi}\left(1+\frac{1-\mu}{1+\mu}\cos(\lambda)\right)^{-1+2/n}\sin(\lambda)\operatorname{cotan}(\tfrac{1}{2}\theta-\tfrac{1}{2}\lambda)\,\mathrm{d}\lambda, \tag{5.1}$$

$$v^{Q}_{t\xi}(\theta)=-\frac{Q}{2\pi n}\frac{\sin(\theta)}{\cos(\theta)+(1+\mu)/(1-\mu)}, \tag{5.2}$$

$$v^{\Gamma}_{t\xi}(\theta)=\frac{\Gamma_1}{2\pi n}\frac{\cos(\theta)+(1-\mu^{\frac{1}{2}})/(1+\mu^{\frac{1}{2}})}{\cos(\theta)+(1+\mu)/(1-\mu)}, \tag{5.3}$$

in which

$$K=\frac{1-\mu}{1+\mu}(\tfrac{1}{2}(1+\mu))^{2/n}\,\Omega r_2^2. \tag{5.4}$$

Equations (5.2) and (5.3) are both simple expressions that need no further explanation. Equation (5.1), however, deserves some further attention. First, substituting the trigonometric identity

$$\operatorname{cotan}(\tfrac{1}{2}\theta-\tfrac{1}{2}\lambda)=\frac{\sin(\lambda)+\sin(\theta)}{\cos(\lambda)-\cos(\theta)} \tag{5.5}$$

and taking into account that the trigonometric function

$$\left(1+\frac{1-\mu}{1+\mu}\cos(\lambda)\right)^{-1+2/n}\frac{\sin(\lambda)\sin(\theta)}{\cos(\lambda)-\cos(\theta)} \tag{5.6}$$

is an odd function of λ, we may write (5.1) as

$$v^{\Omega}_{t\xi}(\theta)=\frac{K}{2\pi n}\int_{-\pi}^{\pi}\left(1+\frac{1-\mu}{1+\mu}\cos(\lambda)\right)^{-1+2/n}\frac{\sin^2(\lambda)}{\cos(\lambda)-\cos(\theta)}\,\mathrm{d}\lambda. \tag{5.7}$$

Then employing some elementary trigonometrical manipulations we can rephrase (5.7) as

$$v^{\Omega}_{t\xi}(\theta)=\frac{K}{2\pi n}(\sin^2(\theta)\,\bar{I}(\theta)+(1-\cos(\theta))\,I_1-\bar{I}_0), \tag{5.8}$$

in which
$$I(\theta) = \oint_{-\pi}^{\pi} \left(1+\frac{1-\mu}{1+\mu}\cos(\lambda)\right)^{-1+2/n} \frac{\mathrm{d}\lambda}{\cos(\lambda)-\cos(\theta)}, \tag{5.9}$$

$$I_0 = \int_{-\pi}^{\pi} \left(1+\frac{1-\mu}{1+\mu}\cos(\lambda)\right)^{-1+2/n} (1+\cos(\lambda))\,\mathrm{d}\lambda, \tag{5.10}$$

$$I_1 = \int_{-\pi}^{\pi} \left(1+\frac{1-\mu}{1+\mu}\cos(\lambda)\right)^{-1+2/n} \mathrm{d}\lambda. \tag{5.11}$$

Equation (5.8) is a mathematically convenient simplification, as will be demonstrated shortly hereafter. The integrals I_0 and I_1 can both be expressed elegantly by a rather familiar special function, namely the (Gauss) hypergeometric function or series. The equivalents of the integrals (5.10) and (5.11) read (see also Gradshteyn & Ryzhik 1980, pp. 389, 384)

$$I_0 = 2\pi(\tfrac{1}{2}(1+\mu))^{1-2/n} F\left(\tfrac{1}{2}, 1-\frac{2}{n}; 2; 1-\mu\right), \tag{5.12}$$

$$I_1 = 2^{6/n}\pi(1+\mu)^{1-2/n}(1+\mu^{\frac{1}{2}})^{-4/n}(\mu^{\frac{1}{2}})^{-1+4/n} F\left(\frac{2}{n}, \frac{2}{n}; 1; \left(\frac{1-\mu^{\frac{1}{2}}}{1+\mu^{\frac{1}{2}}}\right)^2\right), \tag{5.13}$$

where $F(-) = {}_2F_1(-)$ represents the (Gauss) hypergeometric function; see for instance Whittaker & Watson (1927).

To evaluate the integral $I(\theta)$ we expand the leading part of integral (5.9) in a Fourier cosine series. The Fourier expansion reads

$$\left(1+\frac{1-\mu}{1+\mu}\cos(\lambda)\right)^{-1+2/n} = \tfrac{1}{2}A_0 + \sum_{k=1}^{\infty} A_k \cos(k\lambda), \tag{5.14}$$

where the coefficients of the series are defined by

$$A_k = \frac{2}{\pi}\int_0^{\pi} \left(1+\frac{1-\mu}{1+\mu}\cos(\tau)\right)^{-1+2/n} \cos(k\tau)\,\mathrm{d}\tau. \tag{5.15}$$

Then substituting (5.14) in (5.9), and using the following principle value integral (Milne-Thomson 1958, p. 80) well-known in aerodynamics:

$$\oint_{-\pi}^{\pi} \frac{\cos(k\lambda)}{\cos(\lambda)-\cos(\theta)}\mathrm{d}\lambda = \frac{2\pi}{\sin(\theta)}\sin(k\theta) \tag{5.16}$$

we obtain
$$I(\theta) = \frac{2\pi}{\sin(\theta)} \sum_{k=1}^{\infty} A_k \sin(k\theta). \tag{5.17}$$

Furthermore, the Fourier coefficients (5.15) can be expressed by the hypergeometric function. It follows that (see also Gradshteyn & Ryzhik 1980, p. 384)

$$A_k = 2^{6/n}(1+\mu)^{1-2/n}(1+\mu^{\frac{1}{2}})^{-4/n}(\mu^{\frac{1}{2}})^{-1+4/n} a_k, \tag{5.18}$$

where
$$a_k = \frac{1}{k!}\left(\frac{1-\mu^{\frac{1}{2}}}{1+\mu^{\frac{1}{2}}}\right)^k F\left(\frac{2}{n}, k+\frac{2}{n}; k+1; \left(\frac{1-\mu^{\frac{1}{2}}}{1+\mu^{\frac{1}{2}}}\right)^2\right) \prod_{m=1}^{k}\left(-m+\frac{2}{n}\right). \tag{5.19}$$

Finally, substituting (5.12), (5.13) and (5.17) in (5.8), and using (5.18), we obtain

$$v_{t\zeta}^{\Omega}(\theta) = -\Omega r_2^2 \frac{1-\mu}{2n} F\left(\tfrac{1}{2}, 1-\frac{2}{n}; 2; 1-\mu\right) + \Omega r_1^2 \frac{1-\mu}{n\mu^{\frac{1}{2}}}\left(\frac{2}{1+\mu^{\frac{1}{2}}}\right)^{4/n}$$
$$\times\left\{\sin(\theta)\sum_{k=1}^{\infty} a_k \sin(k\theta) + \sin^2(\tfrac{1}{2}\theta) F\left(\frac{2}{n}, \frac{2}{n}; 1; \left(\frac{1-\mu^{\frac{1}{2}}}{1+\mu^{\frac{1}{2}}}\right)^2\right)\right\}. \tag{5.20}$$

Equation (5.20) gives the solution in closed form for the fluid velocity, tangential at the unit circle in the ζ-plane, due to the rotation of the impeller. Summing the individual contributions (5.2), (5.3), and (5.20) we get the overall velocity in the ζ-plane. The corresponding velocity in the physical plane is readily obtained by transformation (4.8), which becomes for straight radial blades (i.e. $\beta = 0$)

$$\frac{v_{tz}}{v_{t\zeta}} = \frac{2n}{(1-\mu)\,r_2}\frac{\{R(\theta)\}^{n-1}}{|\sin(\theta)|}, \tag{5.21}$$

where $R(\theta)$ is given by (3.6).

5.1. *Solutions for pump impellers*

From (4.22), (5.2), (5.3), and (5.20) we readily obtain that the blade circulation for pump impellers fitted with straight radial blades is given by

$$n\Gamma_{bp} = \sigma_{p\Omega}\,2\pi\Omega r_2^2 - \sigma_{p\Gamma}\Gamma_1, \tag{5.22}$$

where

$$\sigma_{p\Omega} = \tfrac{1}{2}(1-\mu)\,F\left(\tfrac{1}{2}, 1-\frac{2}{n}; 2; 1-\mu\right), \tag{5.23}$$

$$\sigma_{p\Gamma} = 1-\mu^{\frac{1}{2}}. \tag{5.24}$$

The dimensionless factors $\sigma_{p\Omega}$ and $\sigma_{p\Gamma}$ are generally known as slip factors. The respective subscripts employed, refer to pump impellers (p), displacement flow (Ω) and vortex flow (Γ). By definition slip factors are always positive and less than 1. They express that the flow is influenced imperfectly due to the finite number of blades; the fluid is said to slip.

Slip factor $\sigma_{p\Omega}$ is commonly mentioned in many text-books or papers on turbomachinery. It represents the rotational slip of the flow due to imperfect guidance of the blades. Slip factor $\sigma_{p\Gamma}$, however, is hardly ever found in the (turbomachine) literature. It represents the slip of the flow leaving pump impellers due to the prerotation at impeller entrance. Both slip factors as well as the concept of slip factors will be further discussed in §7.

Next summing (4.20), (5.2), (5.3), and (5.20), and using (5.22), we obtain the overall velocity along the unit circle in the ζ-plane for the pump impeller:

$$v_{t\zeta}(\theta) = -\frac{\sin(\theta)}{\cos(\theta)+(1+\mu)/(1-\mu)}\frac{Q}{2\pi n} - \mu^{\frac{1}{2}}\frac{1-\cos(\theta)}{\cos(\theta)+(1+\mu)/(1-\mu)}\frac{\Gamma_1}{2\pi n}$$
$$+\Omega r_1^2\frac{1-\mu}{n\mu^{\frac{1}{2}}}\left(\frac{2}{1+\mu^{\frac{1}{2}}}\right)^{4/n}\left\{\sin(\theta)\sum_{k=1}^{\infty}a_k\sin(k\theta) + \sin^2(\tfrac{1}{2}\theta)\,F\left(\frac{2}{n},\frac{2}{n};1;\left(\frac{1-\mu^{\frac{1}{2}}}{1+\mu^{\frac{1}{2}}}\right)^2\right)\right\}. \tag{5.25}$$

Then employing transformation (5.21), and using the auxiliary relations (straight radial blades only) $v_{tz}^{+} = -w_r$ and $v_{tz}^{-} = +w_r$, where the superscripts $(+)$ and $(-)$ refer to the upper and lower blade surfaces respectively, we get

$$w_{rp} = \frac{Q}{2\pi r} + \mu^{\frac{1}{2}}\tan(\tfrac{1}{2}\theta)\frac{\Gamma_1}{2\pi r} - \{R(\theta)\}^{n-1}\frac{2\Omega r_1^2}{r_2\mu^{\frac{1}{2}}}\left(\frac{2}{1+\mu^{\frac{1}{2}}}\right)^{4/n}$$
$$\times\left\{\sum_{k=1}^{\infty}a_k\sin(k\theta) + \tfrac{1}{2}\tan(\tfrac{1}{2}\theta)\,F\left(\frac{2}{n},\frac{2}{n};1;\left(\frac{1-\mu^{\frac{1}{2}}}{1+\mu^{\frac{1}{2}}}\right)^2\right)\right\}, \tag{5.26}$$

in which w_{rp} is the outward-directed, relative, *radial* fluid velocity at the blades of the

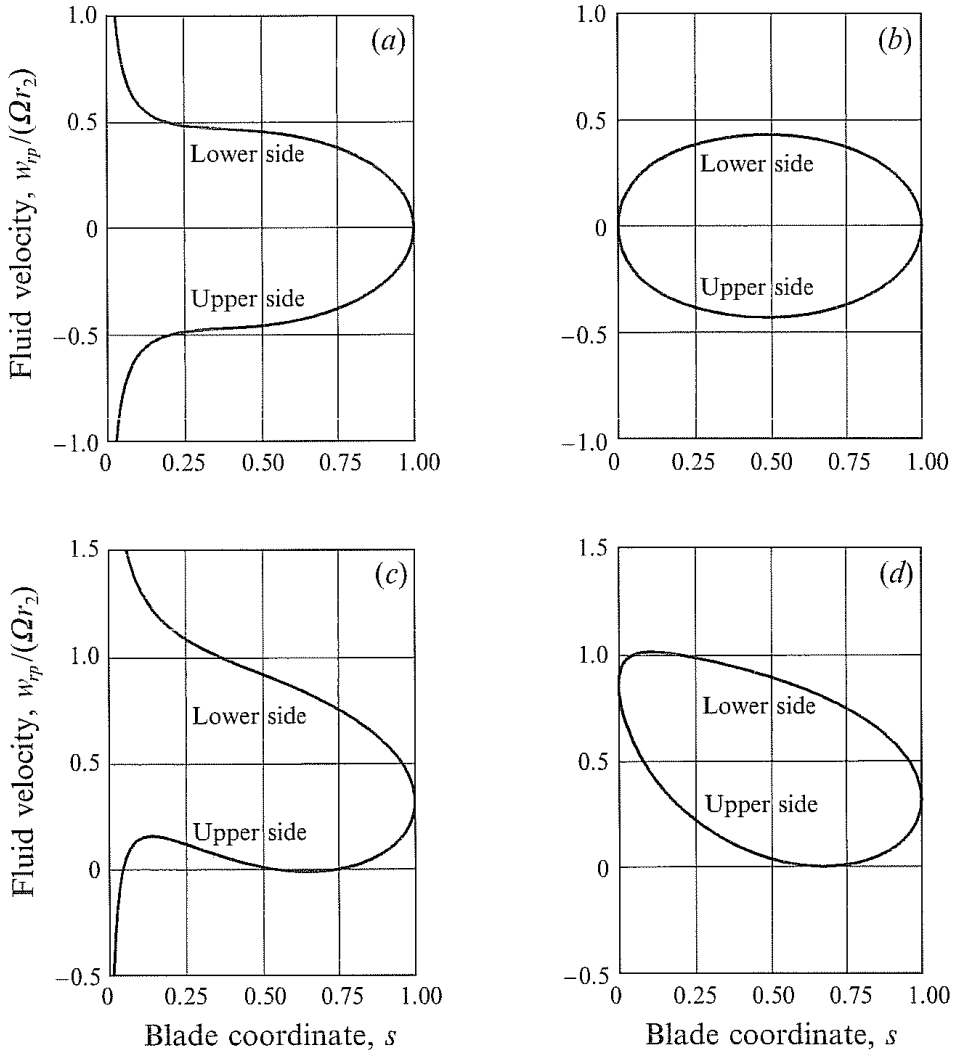

FIGURE 5. Exact solution of fluid velocities along straight radial blades of eight-bladed pump impellers with inlet-to-outlet radius ratio of 0.37 ($\Phi_m = 0.319$; $\Upsilon_{1s} = 0.214$). (*a*) Zero volume flow rate and zero prerotation; (*b*) zero volume flow rate and shockless entry; (*c*) minimum volume flow rate and zero prerotation; (*d*) minimum volume flow rate and shockless entry.

pump impeller, and $r(\theta) = r_2 R(\theta)$ as given by (3.7). For convenience we may rephrase (5.26) in a dimensionless form as

$$R(\theta)\frac{W_{rp}}{\Omega r_2} = \Phi + \mu^{\frac{1}{2}+2/n}\tan(\tfrac{1}{2}\theta)\,\Upsilon_1 - 2\{R(\theta)\}^n\,\mu^{-\frac{1}{2}+2/n}\left(\frac{2}{1+\mu^{\frac{1}{2}}}\right)^{4/n}$$
$$\times\left\{\sum_{k=1}^{\infty} a_k \sin(k\theta) + \tfrac{1}{2}\tan(\tfrac{1}{2}\theta)\,F\left(\frac{2}{n},\frac{2}{n};1;\left(\frac{1-\mu^{\frac{1}{2}}}{1+\mu^{\frac{1}{2}}}\right)^2\right)\right\}, \quad (5.27)$$

where we have introduced a flow coefficient $\Phi = Q/(2\pi\Omega r_2^2)$, and a vortex coefficient $\Upsilon_1 = \Gamma_1/(2\pi\Omega r_1^2)$; both coefficients Φ and Υ_1 may be chosen at will, though the following points should be noted.

Firstly, the flow coefficient Φ, i.e. the throughput in proportion to the rotational speed, should be large enough so that the relative fluid velocity along the impeller blades will be strictly positive, that is $w_{rp} \geqslant 0$. In that case we will not need to take into account the occurrence of reverse flow (i.e. $w_{rp} < 0$), which may have a negative influence on the performance of pump impellers.

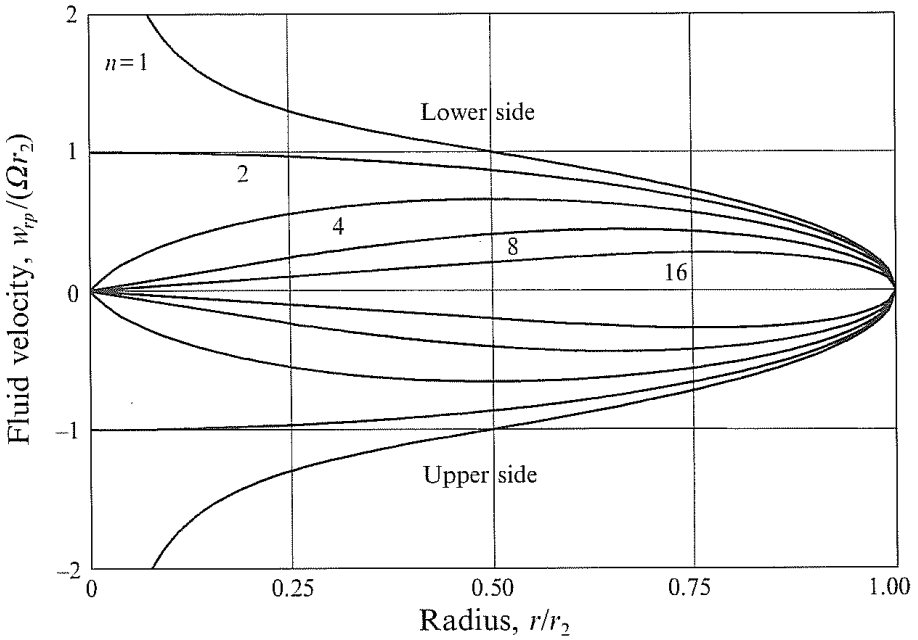

FIGURE 6. Displacement-flow fluid velocity along straight radial blades as $\mu \to 0$.

Secondly, the vortex coefficient Y_1 should preferably be chosen such that a shockless entry is obtained, so that impact losses are reduced to a minimum. From (4.27), (5.2), (5.3), and (5.25), putting $\theta_1 = \pi$, it follows that the prerotation (Γ_{1s}) required to obtain a shockless entry equals

$$\Gamma_{1s} = \tau_p 2\pi\Omega r_1^2 \tag{5.28}$$

or, in dimensionless form,

$$Y_{1s} = \tau_p, \tag{5.29}$$

where we have introduced the prerotation factor τ_p for *pump* impellers, which reads (for straight radial blades)

$$\tau_p = \left(\frac{2}{1+\mu^{\frac{1}{2}}}\right)^{4/n} F\left(\frac{2}{n}, \frac{2}{n}; 1; \left(\frac{1-\mu^{\frac{1}{2}}}{1+\mu^{\frac{1}{2}}}\right)^2\right). \tag{5.30}$$

Like the slip factor the prerotation factor is also dimensionless, but larger than 1.

Both the flow coefficient minimally required to avoid reverse flow, and the prerotation (factor) required for shockless entry will be discussed in greater detail in §7.

To illustrate (5.27) we have plotted in figure 5 the dimensionless fluid velocity $w_{rp}/(\Omega r_2)$ for zero and minimum throughput, both with zero prerotation and shockless entry, for pump impellers with eight straight radial blades and inlet-to-outlet radius ratio $r_1/r_2 = 0.37$. For convenience we here have introduced a dimensionless blade coordinate $s \in [0, 1]$, defined by $s = (r-r_1)/(r_2-r_1) = (R(\theta)-r_1/r_2)/(1-r_1/r_2)$.

Furthermore, we have plotted in figure 6 the asymptotic solution for the displacement flow velocity along straight radial blades as $\mu \to 0$. This solution, i.e. the asymptotic expansion of (5.27), reads

$$R(\theta)\frac{w_{rp}}{\Omega r_2} \sim \Phi - 2^{1-4/n}\Gamma\left(1+\frac{4}{n}\right)\sum_{k=1}^{\infty}\frac{\sin(k\theta)}{\Gamma(1+k+2/n)\,\Gamma(1-k+2/n)} \tag{5.31}$$

as $\mu \to 0$, in which $\Gamma(-)$ represents the well-known (complete) gamma function, and where $R(\theta) \sim \cos^{2/n}(\frac{1}{2}\theta)$ as $\mu \to 0$ which readily follows from (3.6), or (3.15) putting $\beta = 0$.

Figure 6 clearly demonstrates that the displacement flow velocity decreases as the number of blades increases. Moreover, since $1/(\Gamma(1-k)) = 0\,\forall k \in \mathbb{N}^+$, it is seen from (5.31) that

$$R(\theta)\frac{w_{rp}}{\Omega r_2} \sim \Phi \tag{5.32a}$$

as $n \to \infty$, complying fully with one-dimensional Eulerian flow theory. Also, note that the series in (5.31) terminates for $n = 1$ and $n = 2$ after two terms and one term respectively.

Furthermore, it is seen from (5.31) that, for $\Phi = 0$,

$$\lim_{R\to 0} \frac{w_{rp}}{\Omega r_2}\bigg|_{\phi=0} \sim \begin{cases} \pm\infty & \text{when} \quad n = 1 \\ \pm 1 & \text{when} \quad n = 2 \\ 0 & \text{when} \quad n > 2 \end{cases} \tag{5.32b}$$

as $\mu \to 0$, which can also be observed from figure 6. But, nonetheless, we still have for all blade numbers, for $\Phi \neq 0$,

$$\lim_{R\to 0} \frac{w_{rp}}{\Omega r_2} \sim +\infty \tag{5.32c}$$

as $\mu \to 0$.

5.2. *Solutions for turbine impellers*

From (4.23), (5.2), (5.3), and (5.20), putting $\theta_1 = \pi$ and using (4.25) we obtain that the blade circulation for turbine impellers fitted with straight radial blades reads

$$n\Gamma_{bt} = \sigma_{t\Gamma}\Gamma_2 - \sigma_{t\Omega} 2\pi\Omega r_1^2, \tag{5.33}$$

where the slip factors introduced are

$$\sigma_{t\Gamma} = 1 - \mu^{\frac{1}{2}}, \tag{5.34}$$

$$\sigma_{t\Omega} = (1-\mu)\left(\frac{2}{1+\mu^{\frac{1}{2}}}\right)^{4/n} F\left(\frac{2}{n},\frac{2}{n};1;\left(\frac{1-\mu^{\frac{1}{2}}}{1+\mu^{\frac{1}{2}}}\right)^2\right) - \tfrac{1}{2}(1-\mu)\,\mu^{\frac{1}{2}-2/n} F\left(\tfrac{1}{2}, 1-\frac{2}{n};2;1-\mu\right). \tag{5.35}$$

Note that $\sigma_{t\Gamma} = \sigma_{p\Gamma}$ and $\sigma_{t\Omega} = (1-\mu)\tau_p - \mu^{\frac{1}{2}-2/n}\sigma_{p\Omega}$.

Next, summing (4.20), (5.2), (5.3), and (5.20), and using (5.33) we get the overall fluid velocity in the ζ-plane:

$$v_{t\zeta}(\theta) = -\frac{\sin(\theta)}{\cos(\theta)+(1+\mu)/(1-\mu)}\frac{Q}{2\pi n} + \frac{1}{\mu^{\frac{1}{2}}}\frac{1+\cos(\theta)}{\cos(\theta)+(1+\mu)/(1-\mu)}\frac{\Gamma_1}{2\pi n}$$
$$+\Omega r_1^2 \frac{1-\mu}{n\mu^{\frac{1}{2}}}\left(\frac{2}{1+\mu^{\frac{1}{2}}}\right)^{4/n}\left\{\sin(\theta)\sum_{k=1}^{\infty} a_k \sin(k\theta) - \cos^2(\tfrac{1}{2}\theta)\,F\left(\frac{2}{n},\frac{2}{n};1;\left(\frac{1-\mu^{\frac{1}{2}}}{1+\mu^{\frac{1}{2}}}\right)^2\right)\right\}. \tag{5.36}$$

Then using transformation (5.21) we obtain, analogously to the solution for the pump impeller, that the *radial* fluid velocity w_{rt} at the blades of the *turbine* impeller is given by

$$w_{rt} = \frac{Q}{2\pi r} - \frac{\operatorname{cotan}(\frac{1}{2}\theta)}{\mu^{\frac{1}{2}}}\frac{\Gamma_1}{2\pi r} - \{R(\theta)\}^{n-1}\frac{2\Omega r_1^2}{r_2\mu^{\frac{1}{2}}}\left(\frac{2}{1+\mu^{\frac{1}{2}}}\right)^{4/n}$$
$$\times\left\{\sum_{k=1}^{\infty} a_k \sin(k\theta) - \tfrac{1}{2}\operatorname{cotan}(\tfrac{1}{2}\theta)\,F\left(\frac{2}{n},\frac{2}{n};1;\left(\frac{1-\mu^{\frac{1}{2}}}{1+\mu^{\frac{1}{2}}}\right)^2\right)\right\}. \tag{5.37}$$

In dimensionless form this yields

$$R(\theta)\frac{w_{rt}}{\Omega r_2} = \Phi - \mu^{-\frac{1}{2}+2/n}\operatorname{cotan}(\tfrac{1}{2}\theta)\,\Upsilon_1 - 2\{R(\theta)\}^n\,\mu^{-\frac{1}{2}+2/n}\left(\frac{2}{1+\mu^{\frac{1}{2}}}\right)^{4/n}$$
$$\times\left\{\sum_{k=1}^{\infty} a_k \sin(k\theta) - \tfrac{1}{2}\operatorname{cotan}(\tfrac{1}{2}\theta)\,F\left(\frac{2}{n},\frac{2}{n};1;\left(\frac{1-\mu^{\frac{1}{2}}}{1+\mu^{\frac{1}{2}}}\right)^2\right)\right\}. \quad (5.38)$$

The vortex strength Γ_1 in (5.37) and Υ_1 in (5.38) are prescribed by

$$\Gamma_1 = (1-\sigma_{t\Gamma})\,\Gamma_2 + \sigma_{t\Omega}\,2\pi\Omega r_1^2, \quad (5.39)$$

which readily follows from (4.25) and (5.33); using dimensionless groups (5.39) becomes

$$\Upsilon_1 = \sigma_{t\Omega} + (1-\sigma_{t\Gamma})\,\mu^{-2/n}\Upsilon_2, \quad (5.40)$$

where $\Upsilon_2 = \Gamma_2/(2\pi\Omega r_2^2)$.

Substituting (5.40) in (5.38) we get, using (5.34)

$$R(\theta)\frac{w_{rt}}{\Omega r_2} = \Phi - \operatorname{cotan}(\tfrac{1}{2}\theta)(\Upsilon_2 + \mu^{-\frac{1}{2}+2/n}\sigma_{t\Omega}) - 2\{R(\theta)\}^n\,\mu^{-\frac{1}{2}+2/n}\left(\frac{2}{1+\mu^{\frac{1}{2}}}\right)^{4/n}$$
$$\times\left\{\sum_{k=1}^{\infty} a_k \sin(k\theta) - \tfrac{1}{2}\operatorname{cotan}(\tfrac{1}{2}\theta)\,F\left(\frac{2}{n},\frac{2}{n};1;\left(\frac{1-\mu^{\frac{1}{2}}}{1+\mu^{\frac{1}{2}}}\right)^2\right)\right\}. \quad (5.41)$$

The prerotation (Γ_{2s}) required for shockless entry follows from (4.25), (4.27), (5.2), (5.3), and (5.20). It reads

$$\Gamma_{2s} = \tau_t\,2\pi\Omega r_2^2 \quad (5.42)$$

or, using dimensionless groups,

$$\Upsilon_{2s} = \tau_t, \quad (5.43)$$

where the (turbine) prerotation factor is given by

$$\tau_t = \mu^{\frac{1}{2}+2/n}\left(\frac{2}{1+\mu^{\frac{1}{2}}}\right)^{4/n} F\left(\frac{2}{n},\frac{2}{n};1;\left(\frac{1-\mu^{\frac{1}{2}}}{1+\mu^{\frac{1}{2}}}\right)^2\right) + \tfrac{1}{2}(1-\mu)\,F\left(\tfrac{1}{2},1-\frac{2}{n};2;1-\mu\right). \quad (5.44)$$

This prerotation factor will be further outlined in §7, there we will also discuss the minimally required throughput, that is, the minimum flow coefficient (Φ_m), for turbine impellers. Incidentally, note that $\tau_t = \mu^{\frac{1}{2}+2/n}\tau_p + \sigma_{p\Omega}$.

To complete this section, we will demonstrate similarity between the flow fields for pump and turbine impellers. Both from (5.27), which is valid for pump impellers, and (5.38), which is valid for turbine impellers, it follows that the relative fluid velocity w_r along straight radial blades of either pump or turbine impellers operating under the condition of shockless entry, i.e. $\Upsilon_1 = \tau_p$ and $\Upsilon_2 = \tau_t$ for pump and turbine impellers respectively, is given in closed form by

$$R(\theta)\frac{w_r}{\Omega r_2} = \Phi - \mu^{-\frac{1}{2}+2/n}\left(\frac{2}{1+\mu^{\frac{1}{2}}}\right)^{4/n}$$
$$\times\left\{2\{R(\theta)\}^n\sum_{k=1}^{\infty} a_k \sin(k\theta) + \tfrac{1}{2}(1-\mu)\sin(\theta)\,F\left(\frac{2}{n},\frac{2}{n};1;\left(\frac{1-\mu^{\frac{1}{2}}}{1+\mu^{\frac{1}{2}}}\right)^2\right)\right\}, \quad (5.45)$$

where the blade radius ratio, $R(\theta)$, and the Fourier coefficients, a_k, are as given before by (3.6) and (5.19) respectively.

Note from (5.45) that at the blade tips (i.e. $\theta = 0$ and $\theta = \pi$) we have that $R(\theta)\,w_r/(\Omega r_2) = \Phi$; the disturbance due to the rotation of the impeller vanishes completely at the blade tips.

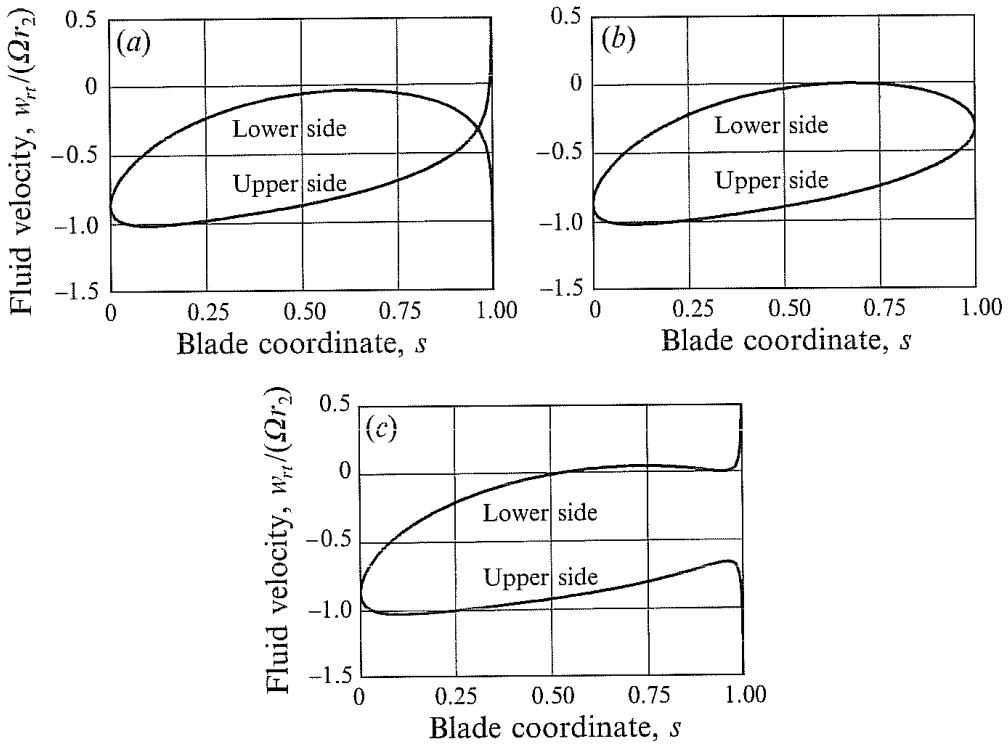

FIGURE 7. Exact solution of fluid velocities along straight radial blades of eight-bladed turbine impellers with inlet-to-outlet radius ratio of 0.37 ($\Phi = -0.319$; $\Upsilon_{2s} = 0.765$). (*a*) Low prerotation ($\Upsilon_2 = 0.9\Upsilon_{2s}$); (*b*) shockless prerotation ($\Upsilon_2 = \Upsilon_{2s}$); (*c*) high prerotation ($\Upsilon_2 = 1.1\Upsilon_{2s}$).

Finally, to illustrate (5.41) we have plotted in figure 7 the dimensionless fluid velocity $w_{rt}/(\Omega r_2)$ for three distinct values of the prerotation, namely 90% of the value required for shockless entry, the value appropriate for shockless entry itself, and 110% of the value corresponding to shockless entry, all with the same volume flow rate (namely $\Phi = -0.319$).

6. Asymptotic solutions for logarithmically bladed pump impellers

In this section pump impellers only will be considered, mainly because solutions in closed form have not yet been obtained for turbine impellers that are fitted with curved blades. This is not of major importance since most radial turbine impellers found in practice have straight radial blades – discussed in detail in the previous section – or are closely represented by these blades, in particular at the entrance section. In fact, blade curvature in radial turbomachines is more commonly applied to pumps and fans.

The solutions presented here give an account of the fluid velocity tangential at the blades of pump impellers fitted with logarithmical spiral blades having a low inlet-to-outlet radius ratio; that is, for the case in which the approximation $\mu = (r_1/r_2)^n \to 0$ is justified.

6.1. *Solutions from the method of conformal mapping*

Analogously to the mathematical treatment given in §5 we are also able to solve the case of logarithmically bladed pump impellers as $\mu \to 0$. We will briefly outline the results.†

† Details of the mathematical manipulations involved are lodged in the JFM office. Anyone wishing to see the details is invited to write to the Editor.

First, it is found that the blade circulation of logarithmically bladed pump impellers is given by

$$n\Gamma_{bp} \sim \sigma_{p\Omega} 2\pi\Omega r_2^2 + Q\tan(\beta) - \Gamma_1 \tag{6.1}$$

as $\mu \to 0$, where the slip factor reads

$$\sigma_{p\Omega} \sim \frac{\mathrm{e}^{-2\beta\sin(2\beta)/n}}{\left(1+\dfrac{4\cos^2(\beta)}{n}\right)(2\cos(\beta))^{4\cos^2(\beta)/n}\, B(\chi,\bar{\chi})} \tag{6.2}$$

as $\mu \to 0$, in which $B(-)$ is beta function (see for instance Abramowitz & Stegun 1972), and where

$$\chi = 1 + \frac{2\cos^2(\beta)}{n} + \mathrm{i}\frac{\sin(2\beta)}{n}. \tag{6.3}$$

Note that χ is a complex number; the beta function $B(\chi,\bar{\chi})$, however, is strictly real valued. The slip factor (6.2) will be further discussed in §7.

Then, taking the blade circulation in accordance with (6.1), it follows that the outwardly directed relative fluid velocity (w_{sp}) tangential at the blades of logarithmically bladed pump impellers is given by, employing a dimensionless notation,

$$R(\theta)\frac{w_{sp}}{\Omega r_2} \sim \frac{\Phi}{\cos(\beta)} - \{R(\theta)\}^2\sin(\beta) - (\cos(\beta))^{-4\cos^2(\beta)/n}\,\mathrm{e}^{-2\beta\sin(2\beta)/n}\operatorname{cotan}(\beta+\tfrac{1}{2}\theta)$$
$$\times\left\{\frac{\sin(2\beta+\frac{1}{2}\theta)}{\cos(\beta+\frac{1}{2}\theta)}\sum_{k=1}^{\infty} B_k\sin(k\theta+2k\beta) - \frac{n}{2\cos(\beta)}\sum_{k=1}^{\infty} kC_k\sin(k\theta+2k\beta)\right\} \tag{6.4}$$

as $\mu \to 0$, in which Φ is the flow coefficient and $R(\theta)$ is the dimensionless radius, as introduced before, and where the Fourier coefficients B_k and C_k are conveniently given as the real and the imaginary parts of the right-hand side of

$$B_k + \mathrm{i}C_k = \frac{2^{1-4\cos^2(\beta)/n}}{(1+(4\cos^2(\beta)/n))\, B(\chi_1^{(k)},\chi_2^{(k)})}, \tag{6.5}$$

in which

$$\chi_1^{(k)} = 1 + k + \frac{2\cos^2(\beta)}{n} - \mathrm{i}\frac{\sin(2\beta)}{n}, \tag{6.6}$$

$$\chi_2^{(k)} = 1 - k + \frac{2\cos^2(\beta)}{n} + \mathrm{i}\frac{\sin(2\beta)}{n}. \tag{6.7}$$

Note that (6.4) readily reduces to (5.31) for the case of straight radial blades (i.e. $\beta = 0$).

Based on (6.4) we have plotted in figure 8 the relative fluid velocity (w_{sp}) due to the rotational speed, that is at zero throughput (i.e. $\Phi = 0$), for several eight-bladed pump impellers. The graphs of this figure are appropriate for both backwardly (i.e. $\Omega < 0$) and forwardly (i.e. $\Omega > 0$) curved blades. The figure clearly shows that the displacement flow velocity diminishes as the blade angle increases. This, and other features, will be discussed further in §7.

6.2. *Solutions from the asymptotic expansion of the Poisson equation*

In addition to the previous section, we shall briefly outline the asymptotic behaviour of the solution for the relative fluid velocity for small blade space–chord ratio impellers. In particular the behaviour in a region located remotely, i.e.

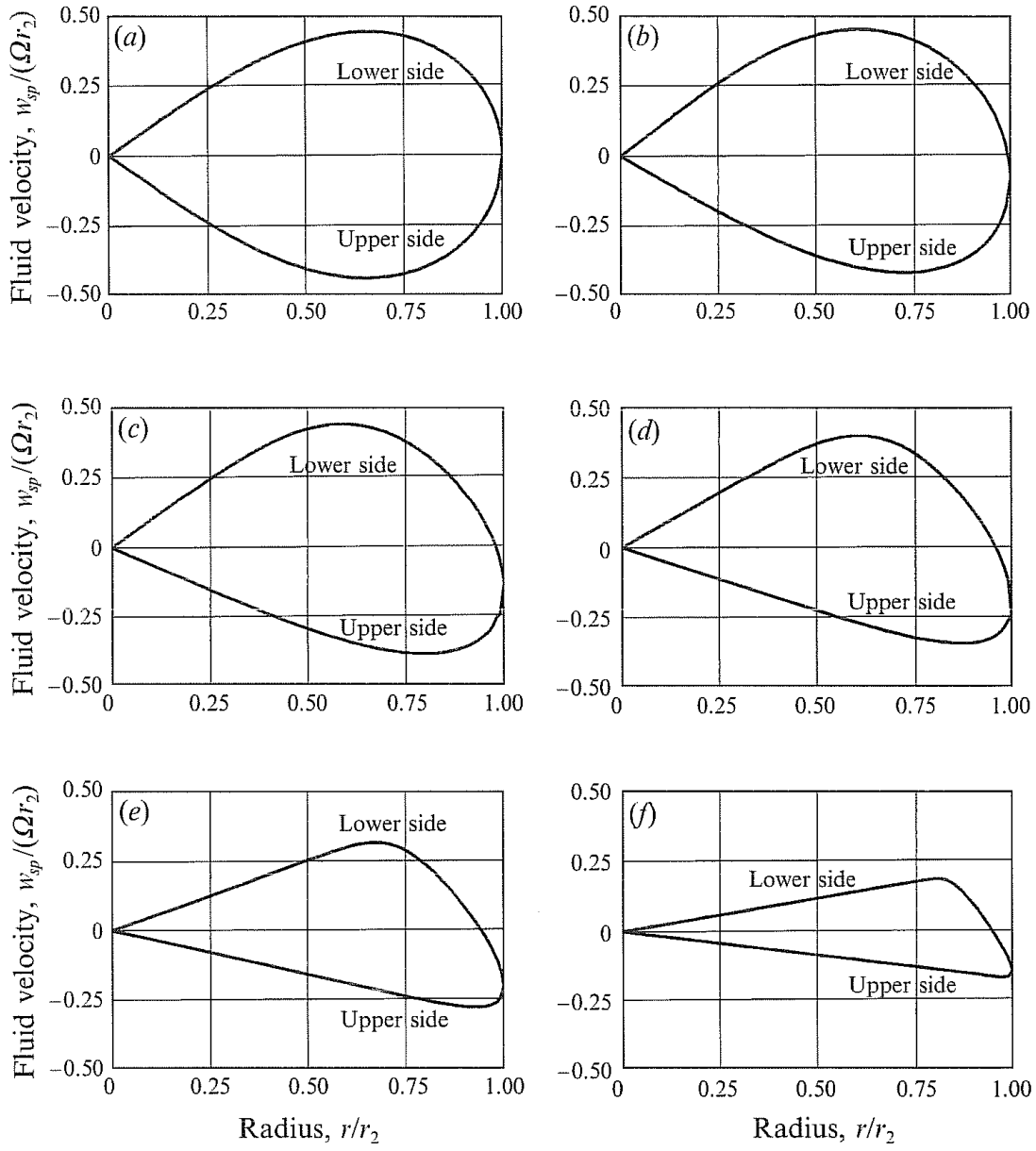

FIGURE 8. Displacement flow velocity along logarithmically curved blades of eight-bladed impellers as $\mu \to 0$. (*a*) $\beta = 0$; (*b*) $\beta = 15°$; (*c*) $\beta = 30°$; (*d*) $\beta = 45°$; (*e*) $\beta = 60°$; (*f*) $\beta = 75°$.

$(1+(2\pi\cos(\beta)/n))\,r_1 \ll r \ll (1-(2\pi\cos(\beta)/n))\,r_2$ with $n/\cos(\beta)$ sufficiently large, between the blade tips of logarithmically bladed impellers will be evaluated. To that end we will consider the Laplacian of the stream function for the relative flow. Unlike the absolute flow, this flow is stationary, and, hence, it is easier to describe than the absolute flow, which is periodical. It will be demonstrated that the asymptotic solution to be given here and the one previously discussed have a striking resemblance.

Denoting the relative stream function by κ, it is found that (see for instance Kucharski 1918, p. 73 or Vavra 1960, p. 226)

$$\nabla^2\kappa = 2\Omega. \tag{6.8}$$

Solving this Poisson equation asymptotically† it follows that the tangential relative

† Details of the mathematical manipulations involved are lodged in the JFM office. Anyone wishing to see the details is invited to write to the Editor.

fluid velocity (w_t) along logarithmic spiral blades, in a region located remotely between the blade tips is given in dimensionless form by

$$\frac{w_t^+}{\Omega r_2} \sim \frac{\Phi}{R\cos(\beta)} + \frac{R}{\sin(\beta)}\left(\frac{\sinh(t)}{t}e^{-t} - 1\right) \tag{6.9}$$

for the upper blade surface, and

$$\frac{w_t^-}{\Omega r_2} \sim \frac{\Phi}{R\cos(\beta)} + \frac{R}{\sin(\beta)}\left(\frac{\sinh(t)}{t}e^{t} - 1\right) \tag{6.10}$$

for the lower blade surface as $\mu \to 0$, in which $R = r/r_2$ and $t = \pi \sin(2\beta)/n$.

Solutions (6.9) and (6.10) agree perfectly with solution (6.4) for $r \ll r_2$ (i.e. $R \ll 1$), which was illustrated in figure 8, the latter being, in fact, the solution for the limiting case $r_1 \to 0$.

From (6.9) and (6.10) we further obtain, restoring physical dimensions,

$$w_t^+ \sim \frac{Q}{2\pi r\cos(\beta)} - \frac{2\pi\Omega r\cos(\beta)}{n}, \tag{6.11}$$

$$w_t^- \sim \frac{Q}{2\pi r\cos(\beta)} + \frac{2\pi\Omega r\cos(\beta)}{n}, \tag{6.12}$$

as $n \to \infty$ (i.e. $t \to 0$).

Equations (6.11) and (6.12) clearly indicate that a negative velocity contribution is to be expected along the pressure side of the blades due to the revolution of the impeller. This is commonly interpreted as being the result of a relative eddy located between consecutive blades, which, basically, originates from the irrotationality of the absolute flow. Consequently, the relative flow possesses a constant vorticity equal to -2Ω (i.e. $\nabla \times w = -2\Omega$).

7. Analytical expressions for impeller design parameters

The solutions given in the previous sections enable the derivation of analytical expressions for parameters which govern the performance of radial impellers in turbomachinery. Parameters concerned are prerotation and condition of shockless entry, delivered head or work, minimum volume flow rate to avoid reverse flow between the blades, pressure distribution along (pump) impeller blades, and dimensions required for impeller housings. Results for each of these parameters are presented below, considering pump and (radially bladed) turbine impellers separately. The findings presented provided an improvement and extension to the design formulae commonly applied in the engineering of radial turbomachinery, such formulae being largely based on the application of one-dimensional Eulerian flow theory.

7.1. *Results for pump impellers*

7.1.1. *Prerotation and condition of shockless entry*

By giving the inlet flow the appropriate prerotation we have the possibility of realizing a shockless entry, for each operating point individually, so that impact losses can be minimized. At this point, however, attention will be confined to impellers fitted with straight radial blades, since only for this type of impeller have solutions in closed form been given with respect to the condition of shockless entry.

From (5.28) we readily obtain the prerotation (Γ_{1s}) required to obtain a shockless

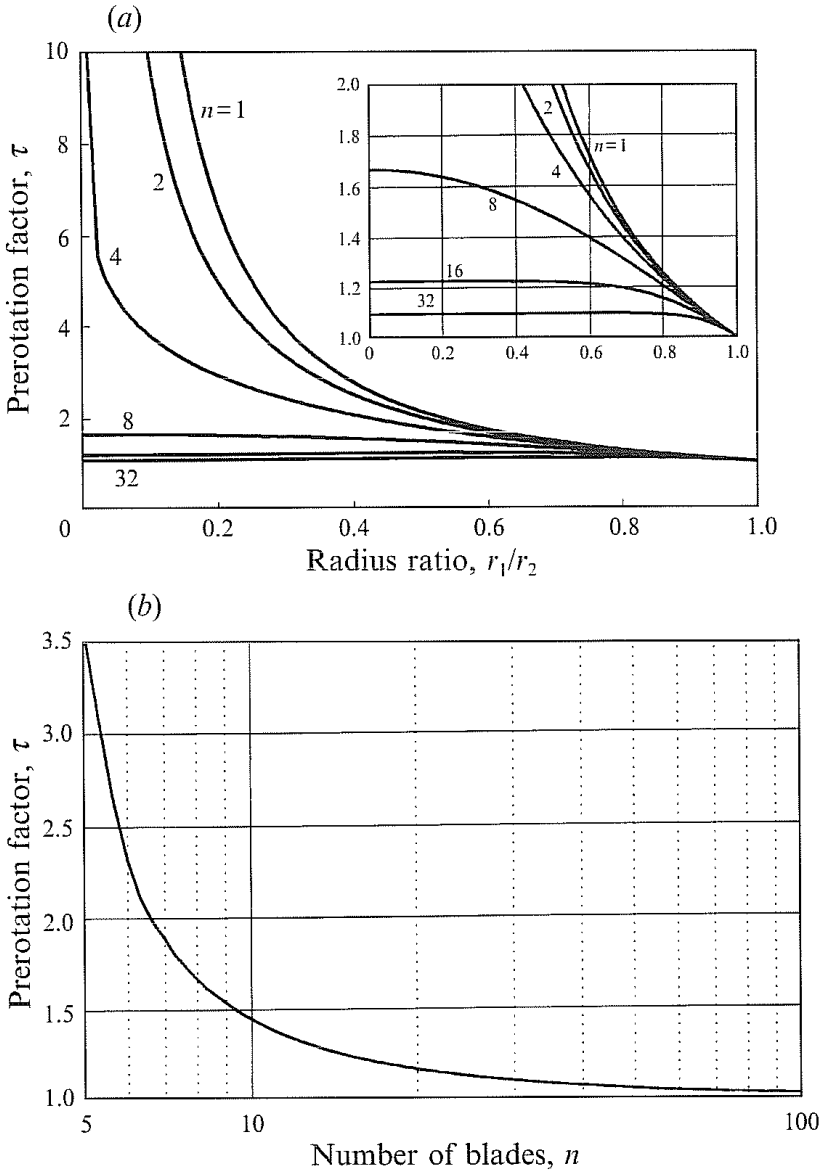

FIGURE 9. Prerotation factor for pump impellers fitted with straight radial blades: (*a*) exact value; (*b*) asymptotic solution as $\mu^{\frac{1}{2}} \to 0$.

entry for pump impellers fitted with straight radial blades, where the prerotation factor is given by (5.30). These equations enable exact evaluation of Γ_{1s}, but, since most impellers are characterized by $\mu \ll 1$ we may approximate asymptotically.

Expanding the prerotation factor readily yields

$$\tau_p \sim 2^{4/n}(1-4\mu^{\frac{1}{2}}/n)\,F(2/n, 2/n; 1; 1-4\mu^{\frac{1}{2}}) \tag{7.1a}$$

as $\mu^{\frac{1}{2}} \to 0$, or

$$\tau_p \sim 2^{4/n}\frac{\Gamma(1-4/n)}{\{\Gamma(1-2/n)\}^2} \tag{7.1b}$$

as $\mu^{\frac{1}{2}} \to 0$, provided that $n > 4$.

The exact value (5.30) and asymptotic expansion (7.1*b*) of the prerotation factor are illustrated in figures 9(*a*) and 9(*b*) respectively. Note that the prerotation factor is always larger than the Eulerian value of unity, and also that when the number of blades becomes infinitely large the prerotation factor becomes unity.

Furthermore, it is noted that, in general, the prerotation for pump impellers (not necessarily the shockless one) is bounded, that is there is a maximum value to be given to the prerotation. This arises from the fact that $n\Gamma_{bp}$ (representing, in fact, the mechanical work transferred to the fluid) has to be positive. With reference to (5.22) and (6.1) we then get the conditions

$$\Gamma_1 < \frac{\sigma_{p\Omega}}{\sigma_{p\Gamma}} 2\pi\Omega r_2^2 \tag{7.2a}$$

for straight radial blades, and

$$\Gamma_1 < \sigma_{p\Omega} 2\pi\Omega r_2^2 + Q\tan(\beta) \tag{7.2b}$$

as $\mu \to 0$, for logarithmic spiral blades.

7.1.2. *Developed head and slip factors*

First, we recollect Euler's turbine equation. For a circular cascade or isolated impeller this may be written conveniently as (see for instance Betz 1966, p. 84)

$$M = \rho Q \frac{\Gamma_2 - \Gamma_1}{2\pi}, \tag{7.3}$$

in which M is torque, or moment, exerted on the impeller and ρ is fluid density. With $\Gamma_2 - \Gamma_1 = n\Gamma_{bp}$ this then gives

$$M = \frac{\rho Q n \Gamma_{bp}}{2\pi} \tag{7.4}$$

for radial-flow pump impellers.

Next assuming 100% efficiency, that is the mechanical work ($M\Omega$) is transferred perfectly to the fluid, we obtain from the conservation of energy that the theoretically developed head (H_{th}) equals

$$H_{th} = \frac{n\Gamma_{bp}}{2\pi g} \tag{7.5}$$

where g is the acceleration due to gravity.

Then substituting (5.22) in (7.5) we get for radially bladed pump impellers

$$gH_{th} = \sigma_{p\Omega}(\Omega r_2)^2 - \frac{\sigma_{p\Gamma}\Gamma_1\Omega}{2\pi} \tag{7.6}$$

or, using dimensionless groups,

$$\Psi_{th} = \sigma_{p\Omega} - (r_1/r_2)^2 \sigma_{p\Gamma} \Upsilon_1, \tag{7.7}$$

in which a head coefficient is introduced, defined by $\Psi_{th} = gH_{th}/(\Omega r_2)^2$; the flow coefficient ($\Phi$), vortex coefficient ($\Upsilon_1$), and slip factors ($\sigma$) are as given before.

Likewise, substituting (6.1) in (7.5) we obtain for pump impellers fitted with logarithmic spiral blades

$$gH_{th} \sim \sigma_{p\Omega}(\Omega r_2)^2 + \frac{Q\tan(\beta) - \Gamma_1}{2\pi}\Omega \tag{7.8}$$

or, in dimensionless form,

$$\Psi_{th} \sim \sigma_{p\Omega} + \Phi\tan(\beta) - \Upsilon_1 \tag{7.9}$$

as $\mu \to 0$.

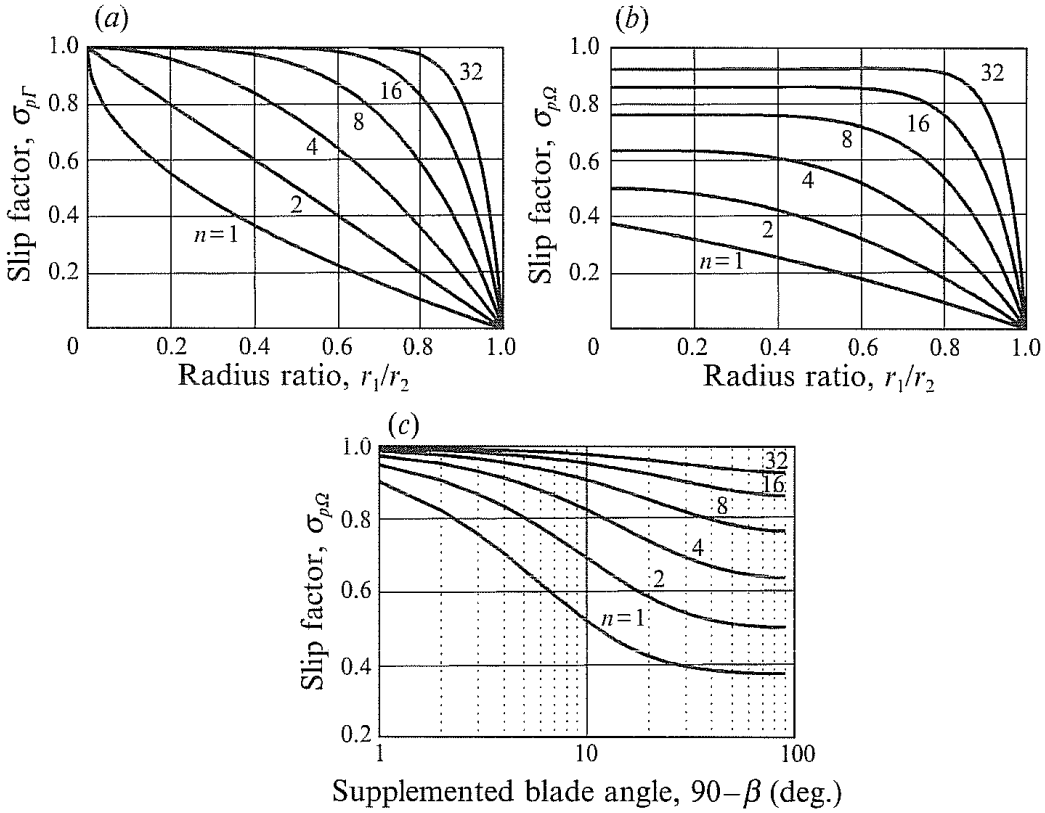

FIGURE 10. Slip factors for pump impellers: (*a*) $\sigma_{p\Gamma}$ for straight radial blades; (*b*) $\sigma_{p\Omega}$ for straight radial blades; (*c*) $\sigma_{p\Omega}$ for logarithmic spiral blades as $\mu \to 0$.

Relations (7.5)–(7.9) clearly illustrate the importance of slip factors. Based on (5.23), (5.24), and (6.2) we have plotted the respective slip factors in figure 10 for several numbers of blades and various blade angles. It shows that increasing the blade angle, as well as the number of blades, will give slip factors closer to the Eulerian value of unity. Consequently, this yields a larger (theoretical) head, as can be seen from (7.5)–(7.9).

Figure 10(*a*) has been given before by Schulz (1928*a*, *b*) and Spannhake (1930). To that end both Schulz and Spannhake derived a solution similar to (5.24). Figures 10(*b*) and 10(*c*) have both been presented formerly by Busemann (1928). Busemann, however, obtained his results by numerical integration, considering a limited number of values for n and β only, whereas figures 10(*b*) and 10(*c*) are based on expressions in closed form, viz. (5.23) and (6.2), enabling direct evaluation for each value of n and β.

Besides slip factors, like the ones just mentioned, another dimensionless group is often also seen in the engineering of turbomachines, namely the head reduction factor (*HRF*). This parameter is commonly defined as the ratio between the theoretical head and the Eulerian head. With (7.7) and (7.9) this gives for straight radial blades (i.e. HRF_0) and logarithmic spiral blades (i.e. HRF_β) respectively

$$HRF_0 = \frac{\sigma_{p\Omega} - (r_1/r_2)^2 \sigma_{p\Gamma} \Upsilon_1}{1 - (r_1/r_2)^2 \Upsilon_1} \tag{7.10}$$

and

$$HRF_\beta \sim \frac{\sigma_{p\Omega} + \Phi \tan(\beta) - (r_1/r_2)^2 \Upsilon_1}{1 + \Phi \tan(\beta) - (r_1/r_2)^2 \Upsilon_1} \tag{7.11}$$

as $\mu \to 0$.

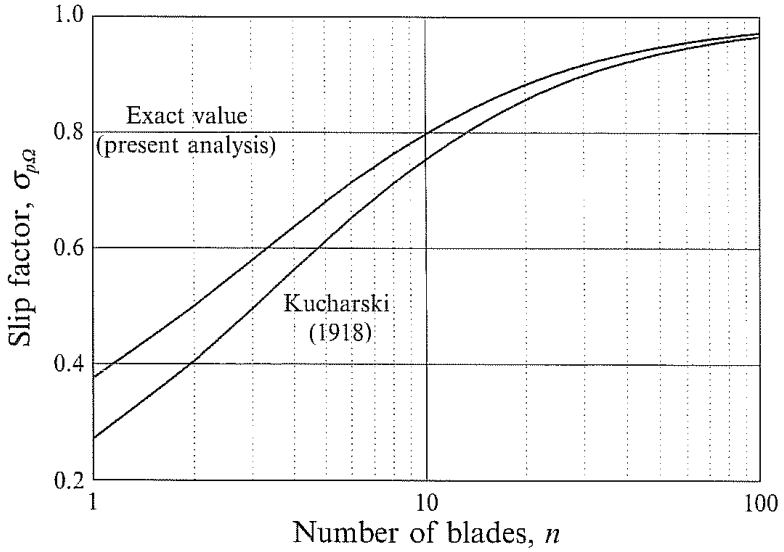

FIGURE 11. Slip factor $\sigma_{p\Omega}$ for pump impellers fitted with straight radial blades as $\mu \to 0$, together with that according to Kucharski (1918).

Equation (7.11) indicates clearly that the head reduction factor is strongly flow-dependent, contrary to the concept of slip factors which depend only on the geometrical design of impellers; hence it is better to use slip factors. Note that the head reduction factor will be equal to the slip factor $\sigma_{p\Omega}$ in the special case of straight radial blades and zero prerotation, i.e. $\beta = 0$ and $\Upsilon_1 = 0$.

Furthermore, referring to (6.3), it is noted that

$$\left(\frac{\mathrm{Im}\{\chi\}}{\mathrm{Re}\{\chi\}}\right)^2 = \left(\frac{(\sin(2\beta))/n}{1+(2\cos^2(\beta))/n}\right)^2 \sim 0 \tag{7.12}$$

as $n \to \infty$, and, consequently, $B(\chi, \bar{\chi}) \sim B(\mathrm{Re}\{\chi\}, \mathrm{Re}\{\chi\}) = \{\Gamma(\mathrm{Re}\{\chi\})\}^2/\Gamma(2\,\mathrm{Re}\{\chi\})$ as $n \to \infty$. Hence, the evaluation of $\sigma_{p\Omega}$ as given by (6.2) can then be simplified to e.g.

$$\sigma_{p\Omega} \sim \frac{1}{\pi^{\frac{1}{2}}} \mathrm{e}^{-2\beta\sin(2\beta))/n} (\cos(\beta))^{-4\cos^2(\beta)/n} \frac{\Gamma(\frac{1}{2}+(2\cos^2(\beta))/n)}{\Gamma(1+(2\cos^2(\beta))/n)} \tag{7.13}$$

as $n \to \infty$. Moreover, in the special case of straight radial blades (i.e. $\beta = 0$) (7.12) holds exactly, and, hence

$$\sigma_{p\Omega} \sim \frac{1}{\pi^{\frac{1}{2}}} \frac{\Gamma(\frac{1}{2}+2/n)}{\Gamma(1+2/n)} \tag{7.14}$$

as $\mu \to 0$, for straight radial blades.

The asymptotic solution (7.14) is plotted in figure 11. In this figure we have also plotted the slip factor $\sigma_{p\Omega}$ according to Kucharski (1918), who has been the only one thus far to formulate solutions in closed form analytically. To that end Kucharski imposed that circular streamlines connected the trailing edges at zero throughput; a simple but remarkably good assumption.

Furthermore, to illustrate (7.9) we have plotted in figure 12 the head coefficient versus the flow coefficient for 60°, logarithmically bladed pump impellers with eight blades, receiving zero prerotation. In this figure we have also plotted the Eulerian head and the actual head as found from measurements (Elholm, Ayder & Braembussche

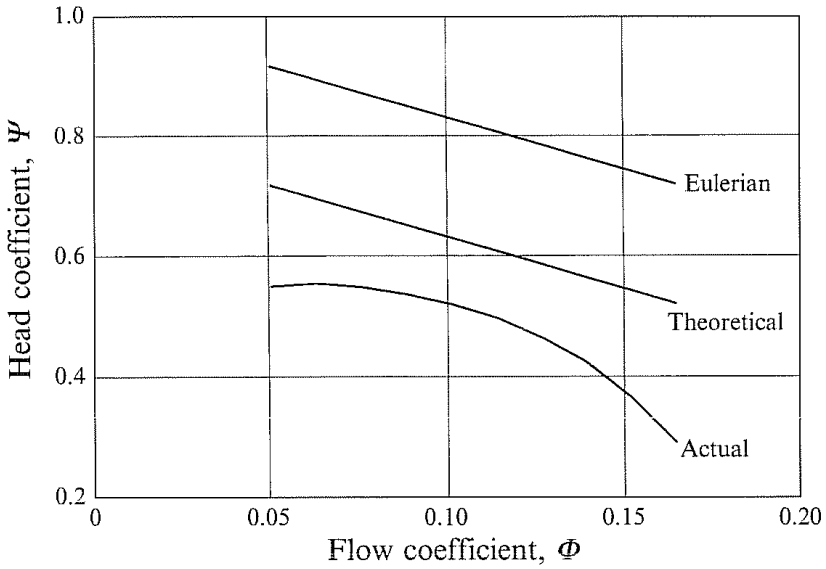

FIGURE 12. Head characteristic for 60°, logarithmically bladed pump impeller with eight blades, having 100 mm outer radius, and receiving zero prerotation.

1992). The figure clearly shows the limiting effect of finite blade numbers. In particular, it shows that the theoretical head lies notably below the Eulerian head. The remaining difference between the theoretical and the actual head is due to friction losses, impact losses, and off-design operation. The latter originates from the fact that the volute does not fit the impeller properly at off-design operation, which will be considered in this section after we have discussed the minimum flow coefficient. The impact losses can simply be reduced by giving the flow entering the impeller the proper prerotation, so that a shockless entry will be obtained.

Lastly, completing the discussion of the subject, it should be noted that not only the references mentioned here, namely Kucharski (1918), Busemann (1928), Schulz (1928*a*, *b*), and Spannhake (1930), have explored the concept of slip occurring in radial impellers. A few others, partially reviewed by Wiesner (1967), have given approximate descriptions for rotational slip; their formulae, however, being mostly based on empiricism.

7.1.3. *Minimum flow coefficient*

Together with slip factors mentioned before we might also have to take into account another, equally important, design parameter, namely the minimum flow coefficient Φ_m. The minimum flow coefficient gives indirectly the lowest allowable throughput, so that there will be no reverse flow between impeller blades. Such reverse flow, expected to have a negative influence on pump performance, arises from the relative vorticity of the flow field (i.e. $\nabla \times w = 2\Omega$), which is related directly to the displacement flow.

From (5.45) and (6.4), with the respective conditions $w_{rp} \geqslant 0$ and $w_{sp} \geqslant 0$ for all radii, it follows that minimum flow coefficients can be computed from

$$\Phi_m\left(n, \frac{r_1}{r_2}\right) = \underset{-\pi<\theta<\pi}{\text{MAX}}\, \mu^{-\frac{1}{2}+2/n}\left(\frac{2}{1+\mu^{\frac{1}{2}}}\right)^{4/n} \times \left\{2\{R(\theta)\}^n \sum_{k=1}^{\infty} a_k \sin(k\theta) + \tfrac{1}{2}(1-\mu)\sin(\theta)\, F\left(\frac{2}{n}, \frac{2}{n}; 1; \left(\frac{1-\mu^{\frac{1}{2}}}{1+\mu^{\frac{1}{2}}}\right)^2\right)\right\} \quad (7.15)$$

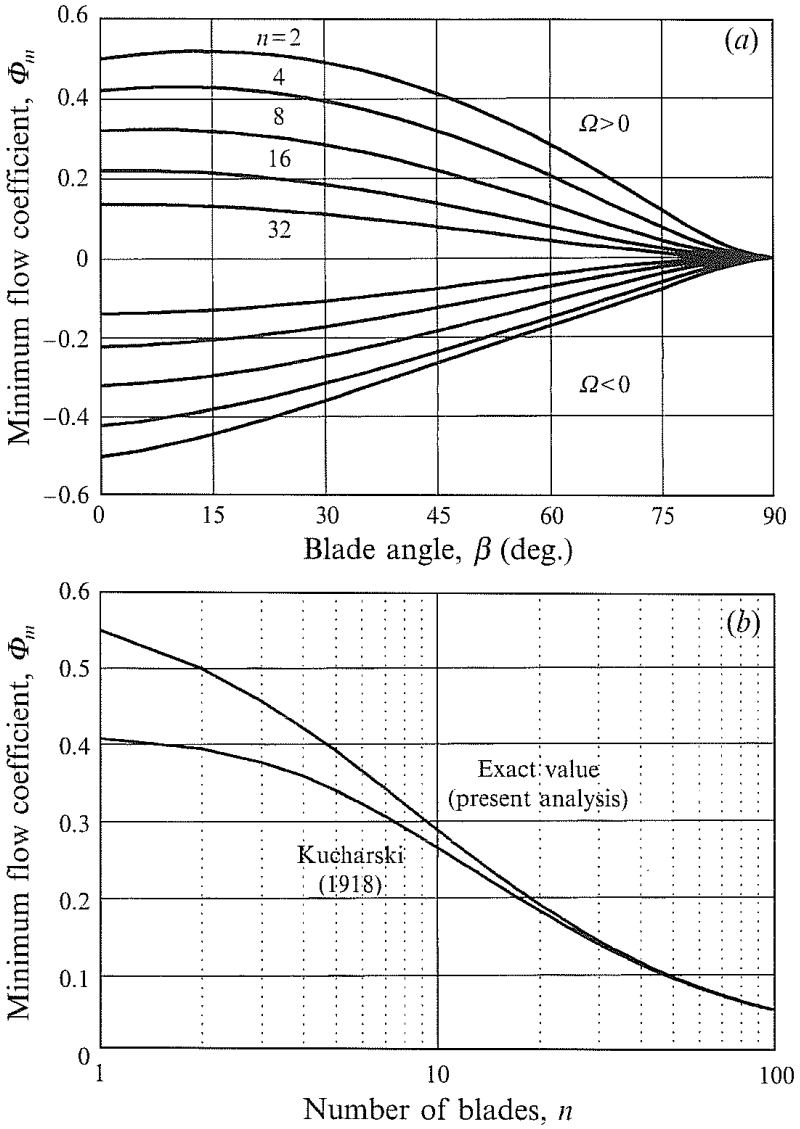

FIGURE 13. Minimum flow coefficient for pump impellers as $\mu \to 0$: (*a*) logarithmical spiral blades; (*b*) straight radial blades.

for straight radial blades, and

$$\Phi_m(n,\beta) \sim \underset{-\pi-2\beta<\theta<\pi-2\beta}{\text{MAX(MIN)}} \tfrac{1}{2}\{R(\theta)\}^2 \sin(2\beta) - (\cos(\beta))^{1-4\cos^2(\beta)/n}\, \mathrm{e}^{-2\beta\sin(2\beta)/n}$$

$$\times \operatorname{cotan}(\beta+\tfrac{1}{2}\theta)\left\{\frac{\sin(2\beta+\tfrac{1}{2}\theta)}{\cos(\beta+\tfrac{1}{2}\theta)}\sum_{k=1}^{\infty} B_k \sin(k\theta+2k\beta) - \frac{n}{2\cos(\beta)}\sum_{k=1}^{\infty} kC_k \sin(k\theta+2k\beta)\right\} \tag{7.16}$$

as $\mu \to 0$, for logarithmical spiral blades, where MAX(MIN) has to be interpreted as MAX if $\Omega > 0$ and as MIN if $\Omega < 0$; the respective dimensionless radii, $R(\theta)$, are given by (3.6) and (3.15) for straight radial and logarithmic spiral blades respectively.

Additionally, putting $\beta = 0$ we readily obtain from (7.16)

$$\Phi_m(n) \sim \underset{-\pi<\theta<\pi}{\text{MAX(MIN)}}\, 2^{1-4/n}\Gamma(1+4/n)\sum_{k=1}^{\infty}\frac{\sin(k\theta)}{\Gamma(1+k+2/n)\,\Gamma(1-k+2/n)} \tag{7.17}$$

as $\mu \to 0$, for straight radial blades, which may also be derived directly using (5.31).

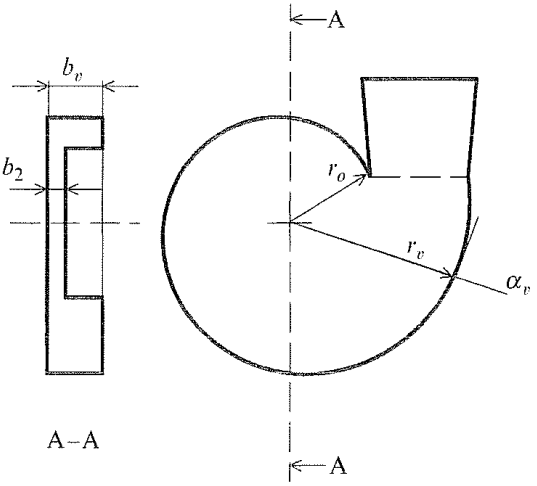

FIGURE 14. Logarithmically curved volute.

The outcome of (7.16) and (7.17) is presented graphically in figure 13, where figure 13(*b*) also shows the minimum flow coefficient as derived by Kucharski (1918). The figure clearly shows the positive effect of curvature; increasing the blade angle and the number of blades will give lower-valued minimum flow coefficients. Logically, the graphs of figure 13 can be used either to determine the lowest allowable volume flow rate or the minimum number of blades and the blade angle required so that reverse flow is avoided.

7.1.4. *Choice of volute*

The findings obtained so far for isolated impellers allow us also to make suggestions about volutes housing pump impellers. To that end we will adapt so-called logarithmically curved volutes, the curvature of which is, like a logarithmical spiral blade, simply described by (see also figure 14)

$$r(\phi) = r_o \, \mathrm{e}^{(\phi-\phi_o)/\tan(\alpha_v)} \tag{7.18}$$

or

$$\phi(r) = \phi_o + \tan(\alpha_v) \ln(r/r_2), \tag{7.19}$$

where α_v is volute angle, ϕ_o is offset angle, and $r_o = r(\phi_o)$.

To compute the volute angle α_v we use the circulation/flux ratio of the flow leaving the impeller. With reference to figure 14 it follows that

$$\tan(\alpha_v) = b_v \Gamma_2/(b_2 Q), \tag{7.20}$$

where b_v/b_2 is depth ratio of the volute.

Next, using (4.25) and substituting respectively (5.22) and (6.1), equation (7.20) gives, employing a dimensionless notation

$$\tan(\alpha_v) = \frac{\sigma_{p\Omega} - (1-\sigma_{p\Gamma})\,\Upsilon_1}{\Phi} \frac{b_v}{b_2} \tag{7.21}$$

for straight radial blades, and

$$\tan(\alpha_v) \sim \left(\frac{\sigma_{p\Omega}}{\Phi} + \tan(\beta)\right) \frac{b_v}{b_2} \tag{7.22}$$

as $\mu \to 0$, for logarithmical spiral blades.

Relations (7.21) and (7.22) provide simple means to compute appropriate volute angles α_v. The depth ratio b_v/b_2 gives the possibility of constructing small volutes, since

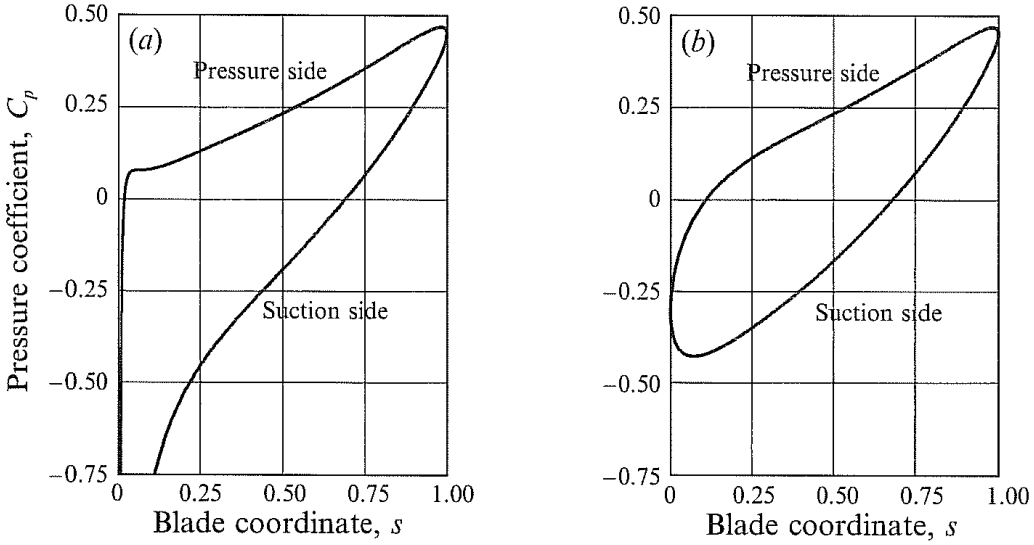

FIGURE 15. Pressure distribution along straight radial blades of eight-bladed impellers with inlet-to-outlet radius ratio of 0.37 ($\Phi_m = 0.319$; $Y_{1s} = 0.214$): (*a*) minimum volume flow rate and zero prerotation; (*b*) minimum volume flow rate and shockless entry.

at unit depth ratio, i.e. $b_v/b_2 = 1$, most volutes would become excessively large. Alternatively, to avoid large volutes, it is possible to use more than one exhaust, since Φ will be reduced inversely proportionally to the number of exhausts (say n_{ex}, so that $\Phi \propto 1/n_{ex}$). Incidentally, the latter also improves the symmetry and periodicity of the volute flow.

Furthermore, (7.21) and (7.22) clearly show that a particular volute will be suited for one operating point only, and, moreover, that the influence of limited blade numbers is incorporated through the appearance of slip factors. Consequently, volutes for finitely bladed pump impellers have to have larger volute angles than those designed according to one-dimensional Eulerian flow theory, where no account is taken of the occurrence of slip and, hence, circumferential fluid velocities are taken too large.

7.1.5. *Pressure distribution along impeller blades*

In the engineering of turbomachinery the pressure distribution along impeller blades plays a significant role. In particular, forces exerted on impellers, blade loading, and cavitation are of interest.

The pressure distribution along the blades of the impellers can be computed immediately from the velocity distribution, using Bernoulli's theorem for steady two-dimensional fluid motions with respect to rotating axes. Neglecting body forces, the theorem reads (see for instance Batchelor 1967, p. 396, or Prandtl 1963, p. 347)

$$p/\rho + \tfrac{1}{2}w^2 - \tfrac{1}{2}(\Omega r)^2 = B, \tag{7.23}$$

in which p is thermodynamic pressure, ρ is fluid density, and B is (often referred to as Bernoulli's) constant.

Introducing dimensionless groups, (7.23) can be written alternatively as

$$C_p + \tfrac{1}{2}C_w^2 - \tfrac{1}{2}R^2 = B^*, \tag{7.24}$$

where $C_p = p/(\rho\Omega^2 r_2^2)$, $C_w = w/(\Omega r_2)$, $R = r/r_2$, and $B^* = B/(\Omega r_2)^2$.

Based on the velocity distributions of figures 5(*c*) and 5(*d*) we have plotted in figures 15(*a*) and 15(*b*) the pressure coefficient C_p versus the blade coordinate s, where we have put $B = 0$ for convenience; the blade coordinate s, employed before, is related to the dimensionless radius R by $R = s + (1-s)\,r_1/r_2$.

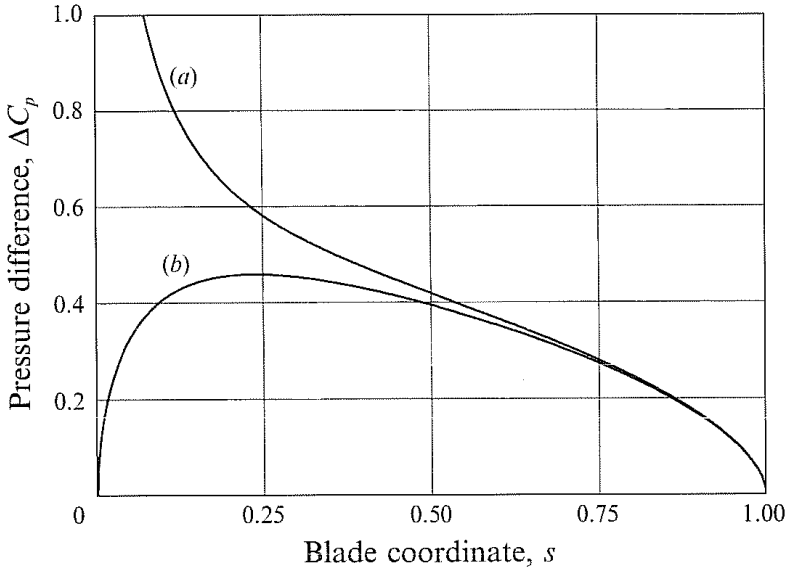

FIGURE 16. Pressure difference over straight radial blades of eight-bladed impellers with inlet-to-outlet radius ratio of 0.37 ($\Phi_m = 0.319$; $\Upsilon_{1s} = 0.214$): (*a*) minimum volume flow rate and zero prerotation; (*b*) minimum volume flow rate and shockless entry.

Figure 15 demonstrates that the blade loading is concentrated near the inner tip, that is the pressure difference ($\Delta C_p = C_p^+ - C_p^-$) over a blade has its maximum near the inner tip. This phenomenon is even better reflected in figure 16, where we have plotted the pressure difference as a function of the blade coordinate.

Also, to illustrate the positive influence of blade curvature with respect to the blade loading, we have computed the pressure distribution along logarithmical spiral blades, based on the velocity distributions of figure 8, with the respective minimum volume flow rate required superposed. The resulting pressure distributions and pressure differences are given in figures 17 and 18 respectively. The figures clearly indicate that blade curvature affects the blade loading favourably.

7.2. *Results for turbine impellers*

7.2.1. *Delivered work and condition of shockless entry*

Employing Euler's turbine equation, e.g. (7.3), it readily follows that the amount of work (P_{th}) theoretically delivered by two-dimensional isolated hydraulic radial-inflow turbine impellers is given by

$$P_{th} = \rho Q \Omega \frac{\Gamma_2}{2\pi} - \rho Q \Omega \frac{\Gamma_1}{2\pi}. \tag{7.25}$$

Here, the outer circulation Γ_2 represents the prerotation. This prerotation strongly determines the work to be delivered by radial-inflow turbine impellers. The inner circulation Γ_1, being related directly to the angular momentum of the fluid at blade inner radius, is merely to be seen as a residual or loss of energy. In practice, however, modern turbine impellers are designed in such a way that this loss of momentum is avoided. This is achieved by curving impeller blades backwardly at the inner radius, or by deviating the flow axially at the impeller inner region and curving the blades appropriately. Although the present two-dimensional analysis is unsuited to specify the blade shapes required at the impeller inner region to accomplish this, in line with practice we set the second term in (7.25) equal to zero, so that

$$P_{th} = \rho Q \Omega \Gamma_2 / 2\pi. \tag{7.26}$$

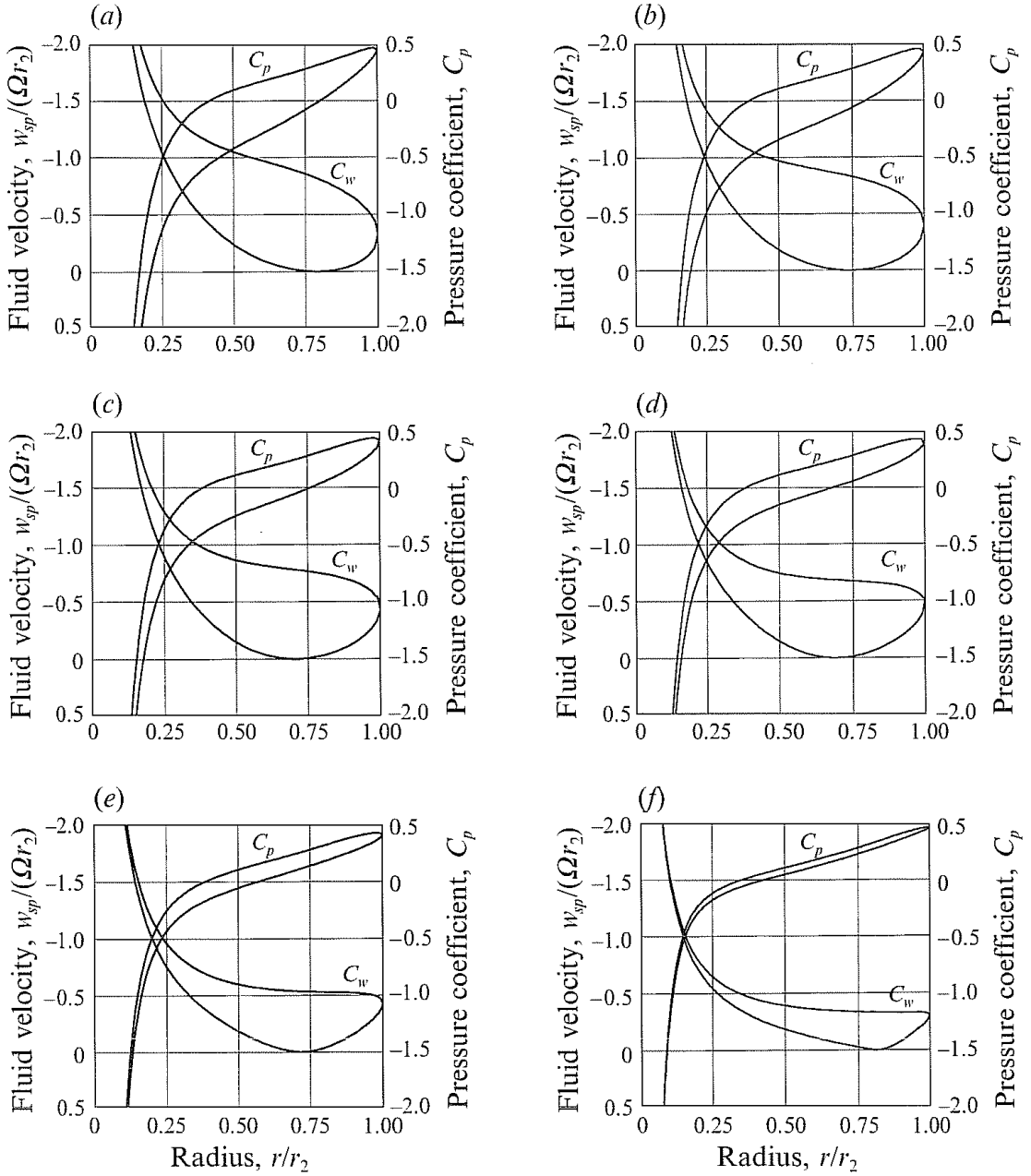

FIGURE 17. Pressure (C_p) and velocity (C_w) distribution at minimum volume flow rate, along backwardly curved logarithmic spiral blades ($\Omega < 0$) of eight-bladed impellers as $\mu \to 0$. (*a*) $\beta = 0$; (*b*) $\beta = 15°$; (*c*) $\beta = 30°$; (*d*) $\beta = 45°$; (*e*) $\beta = 60°$; (*f*) $\beta = 75°$.

Furthermore, to avoid impact losses, turbine impellers are usually operated under the condition of shockless entry. The prerotation Γ_{2s} then required is prescribed by (5.42), which yields, after substitution in (7.26), for the amount of work delivered at shockless entry

$$P_{th,s} = \tau_t \rho Q \Omega^2 r_2^2, \tag{7.27}$$

in which the prerotation factor (τ_t) is prescribed by (5.44), which can be expanded asymptotically for the limiting case of $\mu^{\frac{1}{2}} \to 0$, yielding

$$\tau_t \sim \frac{1}{\pi^{\frac{1}{2}}} \frac{\Gamma(\frac{1}{2}+2/n)}{\Gamma(1+2/n)} \tag{7.28}$$

as $\mu^{\frac{1}{2}} \to 0$.

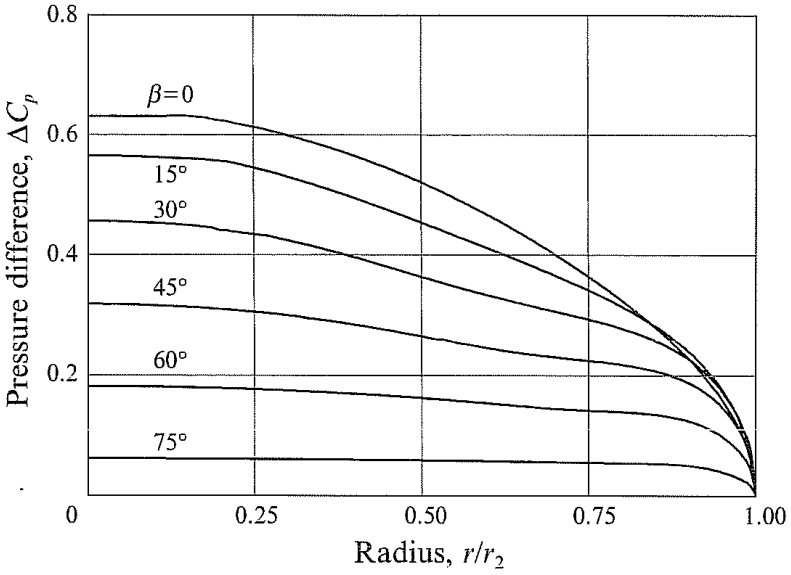

FIGURE 18. Pressure difference at minimum volume flow rate, over backwardly curved logarithmic spiral blades ($\Omega < 0$) of eight-bladed impellers as $\mu \to 0$.

Equation (7.28) provides a simple expression to compute the prerotation required for shockless entry. Figure 19(*b*) shows this prerotation factor as function of the number of blades. The exact value according to (5.44) is plotted in figure 19(*a*). Differences between the exact value and asymptotic expansion of τ_t, as depicted on the graphs of figure 19, reflect the influence of the centre configuration of the turbine impellers on the prerotation required to obtain shockless entry at the impeller outer radius.

In practice, as stated before, blades of radial-inflow turbine impellers are usually curved at the centre or impeller outlet region. As long as this interior part is located in a region of radial extent r_1 such that μ is small, this section is not likely to have much influence on the condition of shockless entry, or on the flow in the impeller inlet region where the blades are actually straight. In that case (7.28) can be applied well to assess the condition of shockless entry.

Lastly, it is noted that the asymptotic expansion of the prerotation factor for shockless entry in radially bladed turbine impellers as given above resembles the slip factor $\sigma_{p\Omega}$ for a radially bladed pump impeller as $\mu \to 0$. Likewise, for finite blade numbers it is smaller than unity, reflecting the remarkable fact – never before noticed (to the authors' knowledge) – that for shockless entry the prerotation of the flow should be less than the one-dimensional Eulerian value derived from the circumferential velocity at the outer blade radius.

7.2.2. *Minimum flow coefficient*

Since (7.15) and (7.17) are also valid for radially bladed turbine impellers, it directly follows that the minimum flow coefficient for radially bladed pump and turbine impellers will be identical. Hence, figure 15 is valid for both type of impellers as $\mu^{\frac{1}{2}} \to 0$. The only difference is that the turbines considered are characterized by radial inward flow, i.e. $Q < 0$, whereas pumps have radial outward flow, i.e. $Q > 0$.

When the throughput lies below the flow minimally required, both turbines and pumps will have reverse flow areas to the pressure side of the blades, located near the

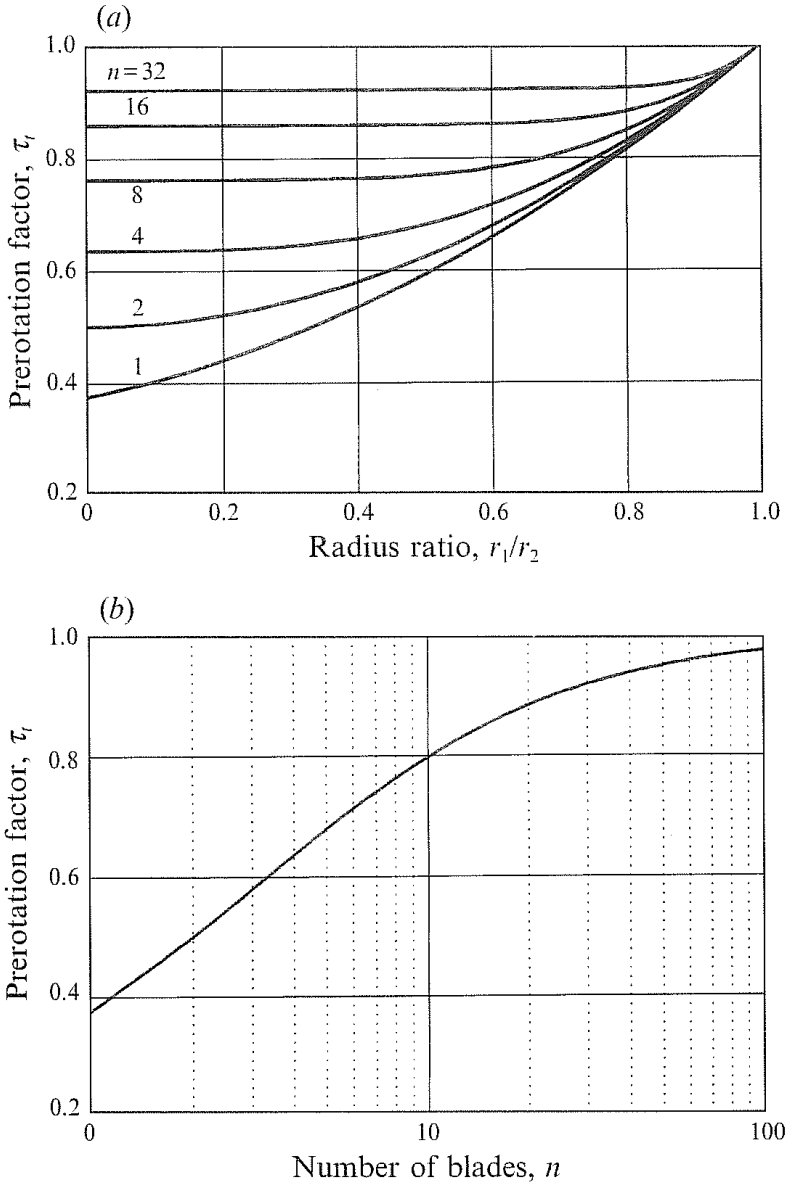

FIGURE 19. Prerotation factor for radially bladed turbine impellers: (*a*) exact value; (*b*) asymptotic solution as $\mu^{\frac{1}{2}} \to 0$. Note that the values for τ_t at $r_1/r_2 = 0$, given in (*a*), are equal to the values of τ_t in (*b*).

outer tip. Logically, this position results from the fact that the throughput velocity is inversely proportional to the radius.

Furthermore, reverse flow will also occur at the leading edge of the blades when the condition of shockless entry is not fulfilled. This is entirely due to the singular behaviour of the velocity profile near the leading edge; see also figures 7(*a*) and 7(*c*).

7.2.3. *Impeller housing*

Assuming a logarithmically spiralled housing, fitted with inlet guide vanes if so desired, we adopt (7.20). Employing dimensionless groups we get (see also figure 14)

$$\tan(\alpha_v) = \frac{b_v \Upsilon_2}{b_2 \Phi}. \tag{7.29}$$

For shockless entry, i.e. $\Upsilon_2 = \tau_t$, which is usually desired, this becomes

$$\tan(\alpha_v) = \frac{b_v \tau_t}{b_2 \Phi}. \tag{7.30}$$

These relations provide a simple means to compute the curvature of radial-inflow turbine impeller housings, so that the flow will be given the desired prerotation. Furthermore, it is clearly shown by both equations that a particular housing will fit one volume flow rate only, since the prerotation factor is determined completely by the design of the impellers.

8. Concluding remarks

In the foregoing the irrotational and solenoidal flow in two-dimensionally modelled, radial-flow impellers fitted with equiangular blades has been analysed in detail. The general approach, including some features of the method of conformal mapping, as well as some of the intermediate or partial results presented, agrees with the works of, notably, Kucharski (1918), Spannhake (1925*a*, *b*, 1930), Busemann (1928), Acosta (1954), and Sörensen (1927, 1941). However, by extending the mathematical analysis, a number of new and previously unpublished results have been derived. These include exact solutions for the velocity distribution along impeller blades of radially bladed pump and turbine impellers, and solutions which hold asymptotically for logarithmically bladed pump impellers as $(r_1/r_2)^n \to 0$, where r_1 is the impeller inner radius, r_2 is the impeller outer radius, and n is the number of blades. The respective solutions have been formulated in closed form, involving Fourier series with Fourier coefficients given by the Gauss hypergeometric function and beta function respectively.

Based on the respective velocity distributions, new or improved expressions have been derived for parameters that are important for practical design of radial turbomachinery, and which reflect the two-dimensional nature of the flow field. In particular, expressions have been given for rotational slip of the flow leaving radial impellers, as well as for reverse flow between impeller blades and shockless flow at impeller entry, with the number of blades, blade curvature, and blade revolution as determinable variables. Furthermore, analytical extensions to classical one-dimensional Eulerian expressions for the developed head of pumps and delivered work of turbines have been given.

Apart from the application to design, the results can serve as a practical reference for complex two- and quasi-three-dimensional, time-dependent, numerical potential flow calculations (Badie 1993). Moreover, they provide a well-defined starting point for further investigation of the flow behaviour in radial-flow impellers, such as boundary-layer calculations along impeller blades employing the potential flow solutions given here for (main-stream) velocity distributions, and experimental observation of situations of reverse flow between impeller blades.

The authors wish to thank Professor L. van Wijngaarden (University of Twente) for his comments on some fundamental issues regarding the application of the method of conformal mapping for two-dimensional problems in fluid mechanics.

REFERENCES

ABRAMOWITZ, M. & STEGUN, I. A. 1972 *Handbook of Mathematical Functions with Formulas, Graphs, and Mathematical Tables*. John Wiley and Sons.

ACOSTA, A. J. 1954 An experimental and theoretical investigation of two-dimensional centrifugal impellers. *Trans. ASME* **76**, 749–763.

AYYUBI, S. B. & RAO, Y. V. N. 1971 Theoretical analysis of flow through two-dimensional centrifugal pump impeller by method of singularities. *Trans. ASME* D: *J. Basic Engng* **93**, 35–41.

BADIE, R. 1993 Analysis of unsteady potential flows in centrifugal pumps. Thesis, University of Twente.

BATCHELOR, G. K. 1967 *An Introduction to Fluid Dynamics*. Cambridge University Press.

BETZ, A. 1964 *Konforme Abbildung*. Springer.

BETZ, A. 1966 *Introduction to the Theory of Flow Machines*. Pergamon.

BUSEMANN, A. 1928 Das Förderhöhenverhältnis radialer Kreiselpumpen mit logaritmisch-spiraligen Schaufeln. *Z. Angew. Math. Mech.* **8**, 372–384.

ELHOLM, T., AYDER, E. & BRAEMBUSSCHE, R. VAN DEN 1992 Experimental study of the swirling flow in the volute of a centrifugal pump. *J. Turbomachinery* **114**, 366–372.

GRADSHTEYN, I. S. & RYZHIK, I. M. 1980 *Table of Integrals, Series, and Products*. Academic.

KÖNIG, E. 1922 Potentialströmung durch Gitter. *Z. Angew. Math. Mech.* **2**, 422–429.

KUCHARSKI, W. 1918 *Strömungen einer reibungsfreien Flüssigkeit bei Rotation fester Körper*. R. Oldenbourg.

LAMB, H. 1932 *Hydrodynamics*. Cambridge University Press.

MILNE-THOMSON, L. M. 1958 *Theoretical Aerodynamics*. Macmillan.

MOHANA KUMAR, T. C. & RAO, Y. V. N. 1977 Theoretical investigation of pressure distribution along the surfaces of a thin blade of arbitrary geometry of a two-dimensional centrifugal pump impeller. *Trans. ASME* I: *J. Fluids Engng* **99**, 531–542.

MORETTI, G. 1964 *Functions of a Complex Variable*. Prentice-Hall.

PFLEIDERER, C. 1991 *Strömungsmaschinen*. Springer.

PRANDTL, L. 1963 *Essentials of Fluid Dynamics*. Blackie and Son.

SCHULZ, W. 1928*a* Das Förderhöhenverhältnis der Kreiselpumpen für die ideale und wirkliche Flüssigkeit. *Forschg. Ing.-Wes.* vol. 307. VDI Verlag.

SCHULZ, W. 1928*b* Das Förderhöhenverhältnis radialer Kreiselpumpen mit logaritmisch-spiraligen Schaufeln. *Z. Angew. Math. Mech.* **8**, 10–17.

SPANNHAKE, W. 1925*a* Die Leistungsaufnahme einer parallelkränzigen Zentrifugalpumpe. *Festschrift der Technische Hochschule Karlsruhe*, pp. 387–400.

SPANNHAKE, W. 1925*b* Anwendung der Konforme Abbildung auf die Berechnung von Strömungen in Kreiselrädern. *Z. Angew. Math. Mech.* **5**, 481–484.

SPANNHAKE, W. 1930 Eine strömungstechnische Aufgabe der Kreiselradforschung und ein Ansatz zu ihrer Lösung. *Mitteillungen des Instituts für Strömungsmaschinen der Technische Hochschule Karlsruhe*, pp. 4–38.

SÖRENSEN, E. 1927 Potentialströmungen durch rotierende Kreiselräder. *Z. Angew Math. Mech.* **7**, 89–106.

SÖRENSEN, E. 1941 Potential flow through centrifugal pumps and turbines. *NACA TM* 973.

UCHIMARU, S. 1925 Experimental research on the distribution of water pressure in a centrifugal impeller. *J. Fac. Engng, Tokyo Imperial University* **16**, 157–169.

UCHIMARU, S. & KITO, S. 1931 On potential flow of water through a centrifugal impeller. *J. Fac. Engng, Tokyo Imperial University* **19**, 191–223.

VAVRA, M. H. 1960 *Aero-Thermodynamics and Flow in Turbomachines*. John Wiley and Sons.

WIESNER, F. J. 1967 A review of slip factors for centrifugal impellers. *Trans. ASME* A: *J. Engng Power* **89**, 558–572.

WHITTAKER, E. T. & WATSON, G. N. 1927 *A Course of Modern Analysis*. Cambridge University Press.